AD-A164 581 X-RAY GENERATED ULTRASOUND(U) CORNELL UNIV ITHACA NY 1/1
DEPT OF THEORETICAL AND APPLIED MECHANICS
W SACHSE ET AL. 30 JAN 86 TAM-TR86-1 N00014-85-K-0263
UNCLASSIFIED F/G 20/1 NL

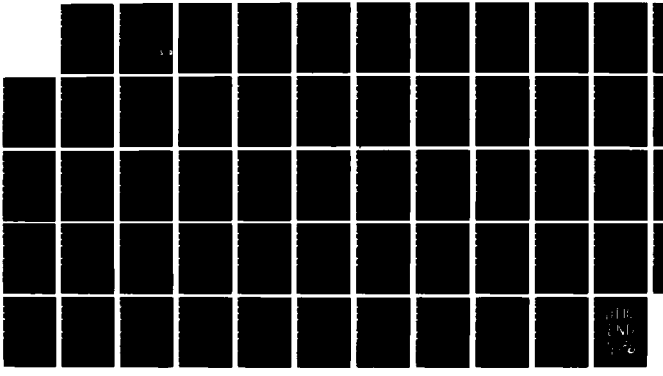

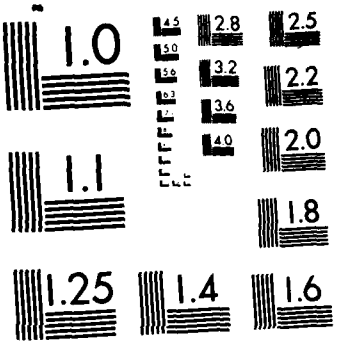

(2)

OFFICE OF NAVAL RESEARCH

SUMMARY REPORT

for

15 April 1985 through 15 January 1986

for

Contract N00014-85-K-0263

Task No. NR 384-940

X-RAY GENERATED ULTRASOUND

Wolfgang Sachse and Kwang Yul Kim

Department of Theoretical and Applied Mechanics
Cornell University
Ithaca, New York 14853

Unclassified

SECURITY CLASSIFICATION OF THIS PAGE (When Data Entered)

REPORT DOCUMENTATION PAGE		READ INSTRUCTIONS BEFORE COMPLETING FORM
1. REPORT NUMBER TAM-TR86-1	2. GOVT ACCESSION NO. AD-A164	3. RECIPIENT'S CATALOG NUMBER 531
4. TITLE (and Subtitle) X-RAY GENERATED ULTRASOUND		5. TYPE OF REPORT & PERIOD COVERED Interim 15 April 1985 - 15 Jan. 1986
		6. PERFORMING ORG. REPORT NUMBER
7. AUTHOR(s) Wolfgang Sachse and Kwang Yul Kim		8. CONTRACT OR GRANT NUMBER(s) N00014-85-K-0263
9. PERFORMING ORGANIZATION NAME AND ADDRESS Cornell University Office of Sponsored Programs 123 Day Hall, Ithaca, New York 14853		10. PROGRAM ELEMENT, PROJECT, TASK AREA & WORK UNIT NUMBERS 61153N 11 NR384-940
11. CONTROLLING OFFICE NAME AND ADDRESS Commanding Officer, U.S. Navy Regional Finance Center CM 3, Room 206, Attn: Code 40, Wash.D.C.20371-5400		12. REPORT DATE 30 January 1986 13. NUMBER OF PAGES 62
14. MONITORING AGENCY NAME & ADDRESS(if different from Controlling Office) Dr. L. E. Hargrove Office of Naval Research 800 North Quincy Street Arlington, Virginia 22217-5000		15. SECURITY CLASS. (of this report) Unclassified 15a. DECLASSIFICATION/DOWNGRADING SCHEDULE

16. DISTRIBUTION STATEMENT (of this Report)

Approved for public release; distribution unlimited

17. DISTRIBUTION STATEMENT (of the abstract entered in Block 20, if different from Report)

18. SUPPLEMENTARY NOTES

19. KEY WORDS (Continue on reverse side if necessary and identify by block number)

x-rays, thermoacoustics, thermal wave imaging, ultrasound, thermal wave

20. ABSTRACT (Continue on reverse side if necessary and identify by block number)

This report describes ~~an investigation of~~ the mechanisms by which ultrasonic signals are generated by an intense, pulsed x-ray source interacting with a material and how the associated contrast mechanisms can be used to image and characterize material microstructures. The existence of x-ray generated acoustic signals was verified and the beam-current dependence

DD FORM 1 JAN 73 1473 EDITION OF 1 NOV 65 IS OBSOLETE
S/N 0102-LF-014-6601

Unclassified

SECURITY CLASSIFICATION OF THIS PAGE (When Data Entered)

of the x-ray generated acoustic signals was established. It was found that the amplitudes of the acoustic signals appear to be linearly related to the electron beam current of the synchrotron and hence the x-ray intensity. Thus, the x-ray/acoustic phenomenon could form the basis of an x-ray beam monitor sensor. The x-ray acoustic signals were also found to depend linearly on the beam size. The generated x-ray/acoustic signals show a directivity pattern resembling that of the thermoelastic signals generated by a pulsed thermal laser source and they appear to be independent of beam width. A newly developed double modulation measurement technique analogous to existing photo-acoustic spectroscopy (PAS) measurements is described. It was found that the x-ray/acoustic spectra are material dependent. Results of X-Y scanning measurements are also reported which were obtained from direct or double-modulated x-ray/acoustic signals recorded as a function of position. It is shown that the measured scanned fields vary spatially, with features apparently related to the effects of the transducer or elastic wave resonances in the specimen. A preliminary test was completed with a new differential x-ray/acoustic measurement technique by which transducer and specimen wave propagation effects were removed so that spatial features in a specimen could be clearly identified.

SUMMARY REPORT

for

Contract N00014-85-K-0263

"X-Ray Generated Ultrasound"

Wolfgang Sachse and Kwang Yul Kim

Cornell University
Ithaca, New York - 14853

1.0 DESCRIPTION OF THE PROBLEM

The focus of this research program is an investigation of the mechanisms by which ultrasonic signals are generated by an intense, pulsed x-ray source interacting with a material and how the associated contrast mechanisms can be used to image and characterize material microstructures.

The recent discovery of x-ray generated ultrasonic signals has lead quite naturally to exploration of the application of these signals to image sub-surface and interior microstructural features in materials. The initial effort in the first year of this project has been towards obtaining a more complete understanding of the x-ray/material interaction processes involved. Both analytical and experimental investigations are being carried out on the phenomenon. The experiments focus on the x-ray, acoustic and material parameters which influence the detected ultrasonic signal amplitudes and contrast mechanisms. The aim of the analytical work is to provide a basis for

an understanding of the x-ray material interaction and the accompanying generation of high-frequency ultrasonic signals.

2.0 APPROACH

In our original proposal, experimental approaches were described in which the interaction process of an x-ray beam and a material was modelled as an assemblage of point sources exponentially distributed through the interior of the material. Adapting the results of Pao, et al. [1], synthetic ultrasonic waveforms could be generated corresponding to various source distributions in plate-like specimens. Also, signal processing algorithms were developed and implemented by Chang [2] by which both the temporal and spatial characteristics of an x-ray/acoustic source could be recovered from the detected signals. It was proposed to use this quantitative ultrasonic measurement procedure as a means of investigating five topics:

1. Dynamic Thermoelastic Sources

2. Characterization of the X-Ray/Material Interaction

3. Imaging by X-Y Scanning

4. Characteristics of X-Ray Generated Ultrasonic Signals

5. The Effects of X-Ray Wavelength

Dynamic thermo-elastic sources were to be studied in a variety of materials and specimen configurations to determine the validity of the extended source modelling approach and the proposed signal inversion scheme by which the spatial distribution of the source and its temporal characteristics could be recovered. In the source characterization studies, the use of quantitative, ultrasonic measurements was to be explored for recovering the average x-ray absorption coefficient of a material. Experiments were also to be carried out to explore the use of such measurements as the basis of a new thermoelastic imaging technique. The existing imaging techniques make use of laser, electron beam or ion beam excitations [3-5]. The beam of x-ray pulses used as a source in this research program differs in several important respects from the thermal sources used heretofore. The time-duration of the pulses comprising the x-ray beam is approximately 160 psec which is two orders of magnitude shorter than the pulsed excitations previously used to generate thermo-elastic or thermal wave signals. Finally, the effect of x-ray energy on the generated ultrasonic signals was to be determined by tuning the synchrotron-generated x-rays with an x-ray monochromator to generate narrowband pulses of x-rays. The aim would be to process the generated acoustic signals to recover the spatial characteristics of the source as a function of x-ray energy and hence, penetration.

Since submission of the original proposal in August 1984, an important modification was made at the Cornell High Energy Synchrotron Source (CHESS) facility where the experiments described here were carried out. This modification has resulted in the generation of three "bunches" of x-ray pulses for every cycle of electrons/positrons in the electron storage ring. Thus,

the pulse repetition frequency is now three times higher than that in our original demonstration experiments, or approximately 800 nsec between excitations. While it was possible in the original experiments to unambiguously identify the various longitudinal and shear wave ray arrivals corresponding to each excitation, in the new operational mode, this was no longer possible. Instead, the x-ray/acoustic signals which are now measured, correspond to a quasi-harmonic excitation having a frequency of about 1.2 MHz. This new development has precluded the identification of the individual wave arrivals and hence also implementation of the detailed signal inversion scheme for recovering the detailed characteristics of the x-ray/acoustic source as originally proposed.

In view of the foregoing, much of the first year's effort has focused on the development of alternate measurement procedures by which each of the five topics originally proposed for investigation could still be studied. This resulted in a new measurement technique which shows great potential. This is a double-modulated x-ray/acoustic spectroscopy technique which appears to provide a means for separating thermal and elastic wave effects in a measured wave field.

In the nine-month period from April through December 1985, the CHESS Facility made six experimentation periods of approximately one week each available to us. In these periods, extensive experiments were completed on topics 1-3 listed above while only preliminary measurements were possible on topics 4 and 5.

3.0 PROGRESS: April 15, 1985 - January 15, 1986

3.1 Verification of the X-Ray/Acoustic Source

In all of the initial experiments related to the discovery of the x-ray/acoustic effect, the piezoelectric detection transducer was mounted at the epicentral receiver position relative to the x-ray target point on the specimen. A critical question to be addressed initially in this research program was related to the possibility that a portion of the transducer output signal was the result of a direct interaction between the x-ray beam and the detecting transducer. To check this, each of the circular, disk-like specimens tested (aluminum, brass, copper, mild steel, stainless steel) was re-tested with a second, point piezoelectric transducer of 1.3 mm diameter mounted on the edge of the specimen, far removed from the direct x-ray beam. Two sample results for aluminum and mild steel are shown in Figures 1 and 2. The results for the other materials are similar.

As shown in these figures and all the others, the acquired waveforms at epicenter and off-epicenter are dominated by the x-ray pulse repetition rate of 1.2 MHz resulting in a quasi-harmonic, periodic output signal. Surprisingly, the amplitudes of the signals detected on the aluminum specimen appear to be lower than those obtained on the steel specimen. But these differences should be accounted for, if the instantaneous synchrotron beam current and hence, the delivered x-ray power, is taken into account and if the transducer/specimen coupling were made identically.

Another noticeable difference between these signals is the apparent phase shift between the epicentral and off-epicentral signals of the aluminum and steel specimens. In aluminum, the phase shift between the epicentral and off-epicentral signals is 224-degrees while for steel the corresponding value is 12-degrees. This effect can be explained from consideration of the phase velocity difference between the aluminum and steel specimens.

3.2 Elastic Wave Propagational Effects

As mentioned above, because of the high source repetition rate, the detailed signal deconvolution procedure originally proposed could no longer be implemented. Experiments were designed to remove the elastic wave propagational effects from the detected signals so that the strength of the source could be recovered, if not its detailed characteristics - distribution and time function. For this, specimens of aluminum, titanium and mild steel were fabricated as shown in Figure 3. These specimens possessed small steps on the front target surface such that if a transducer of sufficiently large diameter was mounted on the back side of the specimen, the detected waveform would exhibit features corresponding to signals propagating over each of the specimen lengths. The intent was to implement a signal analysis technique similar to that described previously by Papadakis, et al. [6].

Measurements were made with two incident x-ray beam widths. The narrow beam, nominally 1.6 x 1.6 mm in cross section, was incident on each section of the specimen in turn as the specimen was moved along a diameter in the beam. Data was taken at thirty points over a 1-1/2 inch length. A typical result

obtained when the rms signal level is measured in the aluminum specimen is shown in Figure 4. The thinner section of the specimen is on the right side of the graph and the signal level is correspondingly higher than that measured for the thicker section. Inspection of the waveforms corresponding to each of the data points measured showed that at some locations, a complicated interference phenomenon existed. The origin of this could not be established and for this reason, a detailed amplitude analysis was not carried out.

An alternate method for using the stepped specimens involves using an incident x-ray beam sufficiently wide, such that all sections of the stepped front surface of the specimen are simultaneously illuminated. In these experiments, the x-ray beam had a cross-section of 1.6 x 30.5 mm. In order to detect the composite signal from all three sections simultaneously, a large receiving transducer was required. Initial measurements were attempted with an X-cut quartz transducer 50 mm in diameter and several PZT broadband transducers, 44 mm in diameter. Unfortunately, the S/N figure of the waveforms detected with each of these transducers was too low to make them useable and for this reason most of the measurements were made with a 1.0 MHz, damped PZT transducer 25 mm in diameter.

The waveforms obtained for each of the specimens tested is shown in Figures 5(a)-(c). Identification of the amplitude values corresponding to particular rays propagating in the specimen is complicated by the pulse superpositioning which occurs because of the low-frequency transducer used and the superimposed noise present. Furthermore, because of the mismatch between the transducer's size and the areas of each of the three steps, the signal

from the central step is expected to be weighted more heavily than the other two areas on either side. For this reason, an amplitude determination of the rays in each section will very likely exhibit large errors. This makes this method of amplitude analysis for recovery of the x-ray/acoustic source amplitude not very promising.

3.3 Thin Film Experiments

In another attempt to separate wave propagational effects from x-ray/acoustic effects in the generated x-ray/acoustic signals to recover the characteristics of the x-ray/acoustic source, a fused silica block specimen was prepared with a sequence of 1000 Å thin-film metal coatings of copper, nickel, gold, aluminum, titanium and tungsten, each 3 mm wide, evaporated on the surface. Using an x-ray beam approximately 1.6 x 1.6 mm in cross-section, the uncoated specimen and each film of the specimen was illuminated in turn and the acoustic signal detected on the back surface with a 18.75 mm diameter 2.25 MHz, damped PZT transducer. Figure 6 is a composite of the waveforms detected for each metal film as well as the case of bare fused silica. Calculation of the decrease in the beam intensity through each of the coatings is tabulated in Table I.

Table I

Metal	μ/ρ	Amplitude Ratio
Al	2.611	.999
Au	11.20	.978
Cu	22.368	.980
Ni	21.238	.981
Ti	12.171	.9945
W	9.861	.981

In attempting to recover the differences of the x-ray/acoustic sources in each of the thin films, a linear systems approach was followed. In this, the frequency spectrum of one cycle of the signals derived from each layer was divided by the corresponding spectrum of the signal obtained from the bare fused silica section. The results showed no clear trend which could be related to a property parameter of the thin films.

In an attempt to obtain an empirical correlation between x-ray/acoustic signal and x-ray/material interaction variables, seven waveform parameters and five material property variables were analyzed. Table II lists these and the derived parameters which were measured.

Table II

Material Property	Waveform Parameter
Elemental Parameters	
Density,	Signal Peak-to-Peak
Thermal Expansion,	Signal maximum
Specific heat,	Signal minimum
Thermal Conductivity,	Signal rms
X-Ray Absorption Coeff.	Signal mean
	Signal energy
	Signal area
Derived Parameters	
Thermal Diffusivity	Various other time
Absolute Absorbed Power	and amplitude features
Thermal Expansion/X-Ray Absorption	extracted from
Thermal Expansion/Density	the waveforms
Thermal Conductivity/X-Ray Absorption	
Others	

As before, no direct correlation could be established between a waveform parameter and any one of the material property parameters. Sample results showing the strongest correlations are given in Figures 7(a)-(h). In each case, while one can identify an expected trend, there are one or more data points which do not follow this trend. There may be two reasons for these observations. One, the differences between the x-ray/acoustic signal from the bare fused silica and a thin-film coated section are so small because of the small differences in the x-ray absorption between the films and the bare silica. And secondly, the spatial variations in sensitivity of the sensor and its coupling characteristics may be as large as the variation in x-ray/acoustic signal differences. However, measurements on specimens as this may give a clearer indication of the source strength in various materials if non-contacting ultrasonic sensors can be successfully utilized to detect the

waveforms.

3.4 Beam Current Dependence

One factor complicating all the x-ray/acoustic measurements is that the beam current of the electron bunches circulating in the storage ring, which is directly related to the x-ray flux, decreases with time. Immediately after a fill, the beam current of the Cornell synchrotron is typically 40 ma decreasing to approximately 18 ma near the end of a 1-1/2 hr run. The incident photon flux correspondingly decreases from 1.30 to 0.59 watts.

To determine the relationship between the beam current and the detected acoustic signals, measurements were made on specimens of brass, copper, mild steel, stainless steel and titanium, while changes in the acoustic waveforms were monitored with decreasing beam current. In the measurements, one hundred acoustic signals were averaged and the rms, peak-to-peak and energy values of the waveforms extracted for each electron beam current value. The results obtained on the stainless steel specimen are shown in Figure 8. It is observed that the decrease in signal rms amplitude is nearly linear with a non-zero intercept. The reason for the latter has not yet been determined. The initial, high-beam current portions of the curves do exhibit an anomalous behavior which appears to be related to tuning operations performed on the beam by the synchrotron operators.

It should also be mentioned that in some cases an anomalous behavior was observed during a run. This was often related to cases in which the signals

were small in amplitude, probably the result of a poor transducer/specimen bond, if the tuning of the x-ray beam was incomplete or if the exit point of the beam from the synchrotron was improperly adjusted.

The results obtained for another stainless steel specimen are shown in Figures 9(a)-(c). The abscissa is given in terms of a voltage with 1.0 volts corresponding to 40 ma of beam current. The last figure shows a jump in the signal output which appears to be related to the operational characteristics of the synchrotron. These observations suggest a possible application of the x-ray/acoustic phenomenon as the basis of an x-ray beam monitor sensor.

The result of one test on brass which spanned a very broad range of beam current is shown in Figure 10. There is no obvious reason for the observed non-linear behavior. This result does not appear to be typical, and another test of this material is planned.

The corresponding results for titanium are shown in Figures 11(a) and (b). The latter gives a record of the signal changes occurring during the tuning of the synchrotron immediately after a run has started. Similar data for the copper and mild steel specimens is shown in Figures 12(a) and (b). The signal-decay curves generated when the peak-to-peak or energy of the waveform is plotted yield similar results. A compilation of the signal rms decay rates and intercepts extracted from what are believed to be the most reliably measured decay curves is listed in Table III. The number in parenthesis following some of the data values indicates the number of tests included in the figure.

Table III

Parameter	Brass	Stainless Steel	Titanium	Copper	Mild Steel
Signal rms Decay rate (mV/beam volts)	83.9	75.9 (2)	91.4 (2)	51.8	90.6 (2)
Intercept (mV rms)	1.2	12.4 (2)	-1.1 (2)	22.4	12.0 (2)

3.5 Beam Size Dependence

The dependence of the x-ray/acoustic signals on the beam size was also determined. To investigate this, two brass plates 0.50 inches thick were used to form a horizontal beam aperture. The plates were mounted on translation stages which could be moved with actuators from a closed position to open more than 30 mm with a reproducibility better than one micron. The vertical extent of the beam was fixed at approximately 2 mm by slits which form an integral part of the beam pipe. Specimens of aluminum and brass were measured with data collected every two mm of aperture both during opening and closing of the aperture.

The rms and peak-to-peak values of the x-ray/acoustic signals generated in a brass specimen are shown in Figures 13(a) and (b). The waveforms were detected with a transducer 18.8 mm in diameter mounted on the back side of the specimen. Immediately apparent is the linear increase in signal amplitude with increasing aperture. As expected, there is no further increase in the signal amplitude when the aperture exceeds the size of the transducer. At

very small apertures there appear to be some non-linearities present which have not yet been investigated. A comparison of the aperture effect on the signal peak-to-peak values of the signals detected with the same transducer in brass and aluminum specimens is shown in Figure 14. Superimposed is the linear, least-square analysis of this data which demonstrates that over most of the aperture range the relation between the generated signal and aperture is linear. The slope obtained for brass is 19.2 mV per mm-aperture while that for aluminum is 14.5 mV per mm-aperture. But these values can be expected to be affected by specimen/transducer coupling effects and by intensity variations of the excitation beam resulting from tuning operations.

From our earlier work on extended acoustic sources in materials it was expected that as the size of the x-ray/acoustic source increases, the generated signals should show evidence of this with a reduction of the risetime [2]. To determine whether this would also appear as the x-ray beam aperture was increased, the waveforms recorded at different apertures were windowed to obtain one cycle and Fourier-transformed. Shown in Figures 15(a)-(d) are the signals measured at two apertures in aluminum, their Fourier magnitudes and unwrapped phase spectra and the phase difference between the signals obtained from x-ray beams collimated through the 4 and 24 mm apertures. The phase spectra are directly related to the phase velocity and group delay of the waveforms [7]. For waves in non-dispersive media, it is believed that information regarding the extent of an acoustic source can be recovered from measurement of these phase spectra.

3.6 Signal Directivity

The directivity of a source of elastic waves is a parameter which gives essential information about the nature of the source and, hopefully, in the x-ray/acoustic case, the nature of the x-ray/material interaction process. For quantitative ultrasonic measurements it is also essential that the source directivity be known so that non-axial waveform amplitude measurements can be properly compensated.

To determine the directivity pattern of the x-ray/acoustic source, a semi-circular specimen of aluminum was fabricated as shown in Figure 16 with seventeen flat areas machined on the circular surface such that small point piezoelectric transducers of 1.3 mm active area could be properly mounted to detect the radiated signals at points equi-distant from the source at 10-degree intervals in the sound field.

To calibrate the system, provision was made for attaching a piezoelectric point transducer operating as a source, at the x-ray source point and detecting the amplitudes as well as the waveform at each of the receiver points. The calibration signal detected at the epicentral (0-degree) receiver position is shown in Figure 17(a). In Figures 17(b)-(k) are shown the signals detected at each of the 10-degree positions on the specimen. It is seen that as in all the other cases, the signals are dominated by the source repetition rate. Furthermore, for particular orientations, specifically at 10, 20 and 30-degrees, there appears a complicated interference phenomenon in the detected signal which was not observed in the calibration experiment. To

determine the directivity pattern, the amplitude of a particular ray arrival should be measured. The high synchrotron pulse repetition rate precludes this since individual ray arrivals are not readily identifiable. For this reason, only the rms-signal amplitude or peak-to-peak values were determined from the waveforms. Because some of the waveforms were small in amplitude and noise corrupted, it was found that the amplitude could be more reliably determined from the spectral magnitude corresponding to the frequency of the source excitation repetition rate, i.e. 1.2 MHz. These amplitudes were scaled by the amplitude of the P-wave arrival signal determined from the calibration test. The results of the directivity so determined for two cases in which the x-ray beam was approximately 2 X 2 mm in cross-section are shown in Figure 18. It is observed that this radiation pattern resembles that of a dipolar point source. These results are similar to those which have been reported by Hutchins, et al. [8] for a focused laser in which the laser is operating as a thermo-elastic source. The large amplitude value found at 80-degrees is not reliable and hence it is not included in the data shown. The amplitude at this angle is a direct result of the small P-wave amplitude measured at this orientation during the calibration test. It is likely that the piezoelectric point transducer used in the calibration test was not operating as a perfect monopolar source type. For comparison, also shown in Figure 18 is the case of a broad x-ray beam having a cross-section of approximately 2 X 15 mm. The essential features are similar to the narrow beam case, but the peak in directivity observed at approximately 50-degrees is much larger.

3.7 Double-Modulated X-Ray/Acoustic Signals

The use of modulated continuous wave thermal sources to generate thermal as well as thermoelastic waves in solids is becoming well established [c.f. 9]. While it was previously predicted that x-rays could be used similarly as a thermal source [10], to the best of our knowledge this has not yet been reported. Given the high x-ray pulse repetition rate at the facility available to us, recovery of details of the x-ray/acoustic source from the generated ultrasonic signals is complicated. To increase the thermal wavelength and hence the penetration depth of the thermal waves, it is possible to superimpose low-frequency (kHz modulation) on the MHz x-ray pulse repetition rate. The experimental system used for doing this is shown in Figure 19. As shown, the system is capable of operating in several modes. In one, the system can record and process real-time, x-ray generated ultrasonic signals detected with a piezoelectric transducer attached to a sample. In that situation, the output of the transducer is amplified and input directly into a processing oscilloscope or waveform recorder. A typical waveform is shown in Figure 20(a) which was synchronized to the x-ray pulse excitation rate. The addition of a beam chopper with a stainless steel blade superimposes a second modulation on the x-ray pulses which is a thousand times lower in frequency. Attempts were made initially to synchronize the second modulation with the x-ray beam, but the stability requirements placed on the mechanical chopper are difficult to meet with existing chopper technology. As depicted in Figure 20(b), approximately a thousand x-ray generated ultrasonic pulses, unsynchronized with the modulation, are in each triangular-shaped modulation cycle. Using an envelope detector and filter, a quasi-periodic

signal is obtained as shown in Figure 20(c), whose frequency is the chopper modulation frequency and whose amplitude is directly related to the amplitude of the x-ray generated acoustic signals. There is also a phase shift of these signals relative to the reference signal obtained from the chopper.

Both magnitude and phase of the detected signal can be recovered with a lock-in amplifier. It is also possible to use the waveform processing oscilloscope to determine various waveform amplitude and time parameters. Data recording and subsequent data processing is facilitated by an attached mini-computer based data acquisition system. By sweeping the modulation frequency, it is possible to generate an x-ray/acoustic signal spectrum, analogous to that determined in photo-acoustic measurements in which the modulation frequency of a continuous thermal source is varied.

It is not yet clear whether the existing theories of thermal waves in solids (e.g. Opsal and Rosencwaig [11]) are applicable to interpret the signals measured with the technique described here. A principal difference is that the beam of x-rays is not continuous, but is rather a sequence of pulses 160 psec in duration with a repetition period of 800 nsec. It is possible that interference phenomena may arise in thin specimen geometries in the detection of thermal and elastic waves for particular source/receiver separations and specimen geometries. Also, since the frequency dependence of the thermal wavelength is proportional to $f^{-\frac{1}{2}}$ while that of the elastic waves is proportional to f^{-1}, such interferences may exhibit a complicated frequency dependence.

A first application of the modulated pulsed x-ray/acoustic technique was to the determination of the magnitude and phase spectra of several metals. The results obtained for a scan of modulation frequency from zero to about 2.75 kHz is shown in Figures 20(a) and (b). We note the reproducibility of the data from five repeat tests performed on a stainless steel specimen. The cross-section of the x-ray beam was approximately 2 x 2 mm but the result of one test performed on a stainless steel specimen with an x-ray beam of broader cross-section gave the results indicated with a dotted line in Figure 21(a). The phase data shown in Figure 21(b) indicate that those materials which exhibit the largest signal magnitudes also undergo the smallest phase change as the beam modulation frequency is swept. The converse also appears to be true.

One experiment was completed in which a steel plug was imbedded in the interior of an aluminum disk 12.5 mm from the front and rear surfaces. Figure 22 shows a comparison of the magnitude spectra between a solid aluminum specimen and the imbedded pin specimen. Unfortunately, because of a beam dump, the data collection of the latter had to be terminated prior to reaching the maximum modulation frequency. Additional experiments with similar specimens are planned to explore the potential and limitations of this new measurement technique.

3.8 X-Y Scanning

An important component of the work planned during the first year of this contract was the collection of x-ray/acoustic signals while spatially scanning

a specimen in the x-ray beam. As with the other experiments planned, it was hoped to recover the x-ray absorption factor by processing the acoustic signals generated during the x-ray/material interaction. It was expected that this interaction would be sensitive to microstructural features of the target material which could be recovered from the ultrasonic signals.

A series of scanning experiments was made in which specimens were scanned in an x-y raster pattern in the x-ray beam which was approximately 2 x 2 mm in cross-section. But since the plan of the original measurements could no longer be followed at the synchrotron facility, at each measurement point, particular waveform parameters, such as peak-to-peak, rms, mean, maximum, minimum, or others were extracted from the waveforms. As depicted in Figure 19, it was possible to record either real-time waveforms or the modulated x-ray/acoustic data during a scan. Extensive software was written for performing the scanning in various patterns, extracting and acquiring up to three waveform parameters from a digital processing oscilloscope and/or recording entire waveforms at pre-selected or at all points along a scan. In addition to scanning the solid specimen and that containing an imbedded steel pin, specimens with intersecting side-drilled holes, a slanted hole, and a hole terminating in the interior were also tested. Also scanned were the stepped-surface specimens and the thin-film coated fused silica specimen described previously in Sections 3.2 and 3.3, respectively. These specimens are shown in Figure 23.

In most of the experiments the ultrasonic signals were detected with either an 18.8 mm or a 1.3 mm diameter, damped PZT transducer mounted at the

epicentral receiver position. Several additional experiments were made with the point sensor mounted on the edge of the specimen. The scanned region typically covered the central 12 x 12 mm or 18 x 18 mm section of the disk although some detailed scans were made along a particular region of interest.

Figures 24 (a)-(c) are the results obtained when the central region of a solid aluminum disk is scanned and the signals detected with the 1.3 mm PZT transducer. Shown in Figure 24(a) is the rms amplitude of the detected x-ray/acoustic signal. Since the specimen is homogeneous, we conclude from the measured sound field that the spatial variation of signal amplitude is either the result of wave propagation or resonance effects in the disk-like specimen or, in view of the pronounced circular symmetry, evidence of the detecting transducer's radiation pattern.

A contour plot of the same data set is shown in Figure 24(b) while a plot of the delay interval of the first peak in the waveform after the synchrotron-derived synchronization pulse is shown in Figure 24(c). The former can be used to quickly extract dimensional features of the acoustic field. The latter can be converted to identify in- and out-of-phase amplitude regions in the scanned field.

Similar results were observed in the double-modulation experiments. An example using the identical measurement situation as before except that the superimposed second modulation was 1.5 kHz is shown in Figures 25(a)-(c). As before, there is a spatial variation of signal amplitude shown in Figure 25(a) which exhibits a circular symmetry. From the contour plot shown in

Figure 25(b), it is seen that the spacing between the central peak and the annular ring is approximately the same as that observed in the earlier test. Thus, despite a significant change in thermal diffusion length, the detected signal is similar, pointing to the conclusion that the measured results are almost entirely due to the elastic wave field of the specimen.

A result, which became immediately apparent after the initial scanning experiments were completed, was the existence of a complicated wave interference phenomenon at particular points in the scanned region. As an example, in Figures 26(a)-(c) are shown the waveforms measured at three points along a scan line. The interference phenomenon appears in the detected waveform as an apparent frequency which is twice that detected at other positions. This is the case for an out-of-phase interference occurring between two superimposed waveforms whose magnitude and phase are varying spatially.

Similar measurements made with a large diameter transducer are shown in Figure 27. There is again an acoustic field with circular symmetry but with less pronounced maxima and minima than was observed with the smaller diameter piezoelectric transducer.

Finally we show in Figure 28(a)-(c) the results obtained when the point piezoelectric transducer is mounted on the edge of the 2.25-inch diameter, disk-like specimen. The complicated interference pattern appears to be the result of an interference between various acoustic wave modes in the specimen. In thin specimens such interferences may arise between the thermal and

acoustic wave modes.

A number of scanned field measurements was made on a series of disk-like specimens of aluminum possessing a variety of machined "flaws". A specimen containing an imbedded steel plug was described in the previous section; seven x-y scans with double-modulation measurements were completed on this specimen. The other specimens fabricated and the number of scanning measurements performed on each are as follows: crossed holes (4); blind hole (2), slanted hole (12) and a stepped specimen (1). As with the solid specimens, the waveform parameter extracted from the real-time acoustic signal or from the detected amplitude envelope of the double-modulation measurements exhibited a complicated spatial behavior which overshadowed any details of the test feature of the specimen. The case of a scan of the slanted hole specimen is shown in Figure 29(a). Here, the x-ray generated acoustic signals were detected at the epicentral position of the specimen with a transducer 18.75 mm in diameter. The data values correspond to the rms signal amplitude of the detected waveforms. A periodicity in the scanned field is apparent in Figure 29(b) which exhibits features related to the spatial sensitivity of the transducer and what appear to be elastic resonances of the specimen.

In every case, the spatial sound fields appear to be dominated by elastic wave propagation effects. At MHz frequencies the thermal wavelength is orders of magnitude smaller than the acoustic wavelength. But in the double-modulation measurements when the modulation frequency is low enough, the thermal wavelength will be long enough to result in an interaction with the fabricated specimen features, to result in an interference with the

thermo-elastically generated signals. Since the piezoelectric detection scheme employed in these experiments detects signals consisting of both thermal and thermoelastic origins, an important future research direction should include experiments for delineating between the thermoelastic and the thermal contributions to the signals.

An alternate approach which has been tried in this research program is a differential method in which x-ray acoustic signals are detected at two modulation frequencies of the pulsed x-ray beam. In this case, the thermal diffusion length changes. If the wavelength of the ultrasonic signals is determined by the repetition rate of the synchrotron, then a ratio of the two scanned fields permits a determination of the change of the spatial thermal field. The results obtained on the slanted hole specimen are shown in Figure 30. In Figures 30(a) and (b) are the scanned fields measured at 500 Hz and at 2.5 kHz, respectively. In the last three lines of the scan made at 500 Hz there was no x-ray beam. As before, it is difficult to perceive in each of these scanned fields features directly related to the slanted interior hole. However, by forming the ratio of these two scanned fields, Figure 30(c) is obtained. Ignoring the region in which there was no beam, the region of the slanted hole is now apparent. Similar results are obtained when the ratio is formed from the data obtained at 500 Hz and 1.5 kHz (Figure 30(d)). This has been the only test of this idea carried out to date. Clearly, additional measurements are warranted to establish this method as a reliable means for using thermally-generated piezoelectrically detected signals to image interior microstructural features in materials.

4.0 CONCLUSIONS

This annual report gives an overview of the research tasks completed from April 15, 1985 through January 15, 1986 on contract N00014-85-K-0263. The specific results described include the following:

1. The existence of x-ray/acoustic signals was verified. Ultrasonic signals were detected with piezoelectric transducers attached to disk-like specimens at epicentral as well as off-epicentral locations, out of the x-ray beam. In every case, the signals exhibited the time characteristics of the x-ray excitation pulses.

2. Attempts were made to eliminate wave propagational effects in the recorded signals. Experiments were completed with stepped specimens in an attempt on separating source and propagation effects in the detected signals. These attempts were not successful. Other experiments were also completed using a specimen of fused silica with metal thin-film layers. The small, measured differences in signal features could not be uniquely correlated with one or more material property parameters of the thin-film.

3. The beam-current dependence of the x-ray generated acoustic signals was established. While the x-ray beam is operating properly, the acoustic signals appear to be linearly related to beam current. The

x-ray/acoustic phenomenon could form the basis of an x-ray beam monitor sensor.

4. The x-ray acoustic signals have been found to depend linearly on the beam size to the extent up to the width of the receiving transducer.

5. The generated x-ray/acoustic signals show a directivity pattern resembling that of the thermoelastic signals generated by a pulsed thermal laser source. The directivity results appear to be independent of beam width.

6. A new double-modulation measurement technique was developed wherein a mechanical chopper is used to modulate the pulsed x-ray beam. Waveform parameters such as rms, amplitude and phase, were measured as a function of beam modulation frequency. It was found that the x-ray/acoustic spectra are material dependent.

7. X-Y scanning measurements were made in which features of the direct or double-modulated x-ray/acoustic signals are recorded as a function of position. Similar results are obtained in both techniques. It was found that the measured scanned fields vary spatially, with features apparently related to the effects of the transducer or elastic wave resonances in

the specimen. A preliminary test was completed with a differential x-ray/acoustic measurement technique by which spatial features in a specimen can be identified.

5.0 REFERENCES

1. A.N. Ceranoglu and Y.H. Pao, "Propagation of Elastic Pulses and Acoustic Emission in a Plate", Trans ASME, 48, 125-147 (1981).

2. C. Chang and W. Sachse, "Analysis of Elastic Wave Signals from an Extended Source in a Plate", J. Acoust. Soc. Am., 77 (4), 1335-1341 (1985).

3. G. Busse, "Imaging with Optically Generated Thermal Waves", IEEE Transactions on Sonics and Ultrasonics, SU-32 (2), 355-364 (1985).

4. G.S. Cargill, III, "Electron-Acoustic Microscopy", Physics Today, 34 (10), 27-32 (1981).

5. J.C. Murphy, J.W. Maclachlan, R.B. Givens, F.G. Satkiewicz and L.C. Aamodt, "The Generation of Ultrasound by Laser, electron and Ion Probes and Its Application to the Characterization of Materials", Proceedings of Ultrasonics International 85, Butterworth Scientific. In Press (1985).

6. E.P. Papdakis, K.A. Fowler and L.D. Lynnworth, "Measurement of Fluid Density", J. Acoust. Soc. Am., 53, 1336-1343 (1973).

7. Y.H. Pao and W. Sachse, "On the Determination of Phase and Group Velocities of Dispersive Waves in Solids", J. Appl. Phys., 48 (8), 4320-4327 (1978).

8. D.A. Hutchins, R.J. Dewhurst and S.B. Palmer, Ultrasonics, 19, 103-108 (1981).

9. "4th International Topical Meeting on Photoacoustic, Thermal and Related Sciences", Ecole Polytechnique de Montreal, August 1985.

10. A. Rosencwaig, Photoacoustics and Photoacoustic Spectroscopy, John Wiley, New York (1980), pp. 297.

11. J. Opsal and A. Rosencwaig, "Thermal Wave Depth Profiling: Theory", J. Appl. Phys., 53, 4240 (1982).

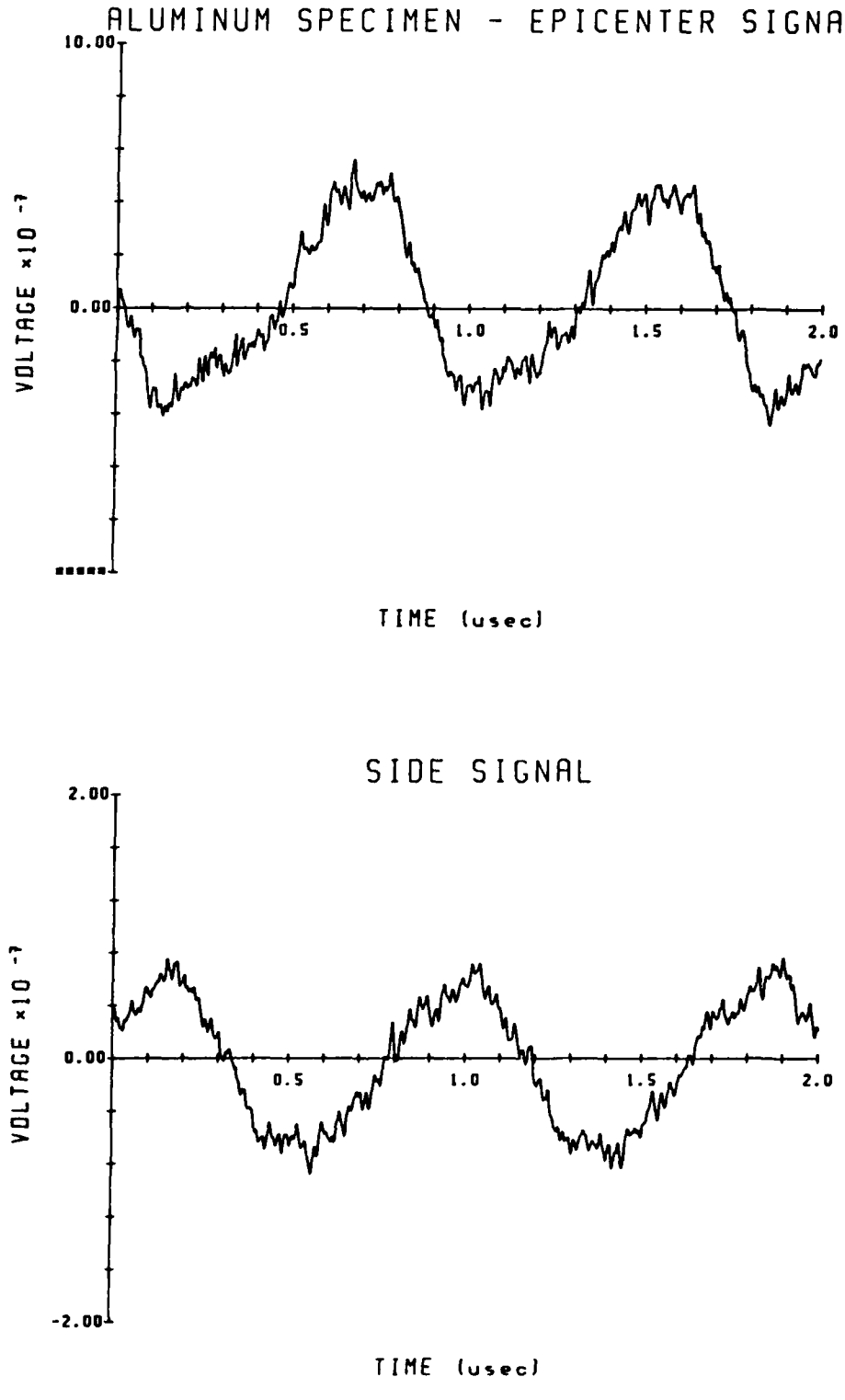

Figure 1 - X-ray/Acoustic Signals in Aluminum

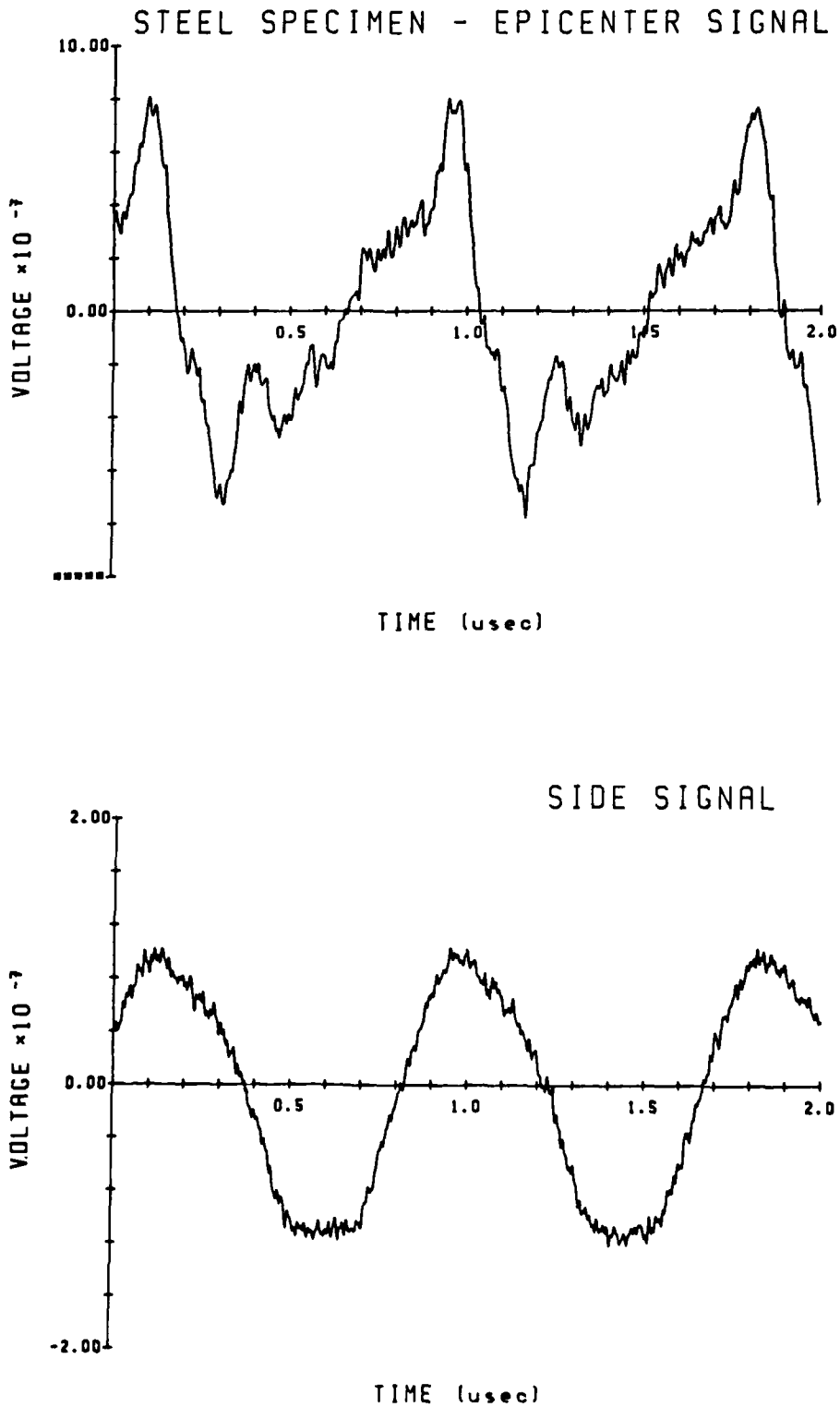

Figure 2 - X-ray/Acoustic Signals in Steel

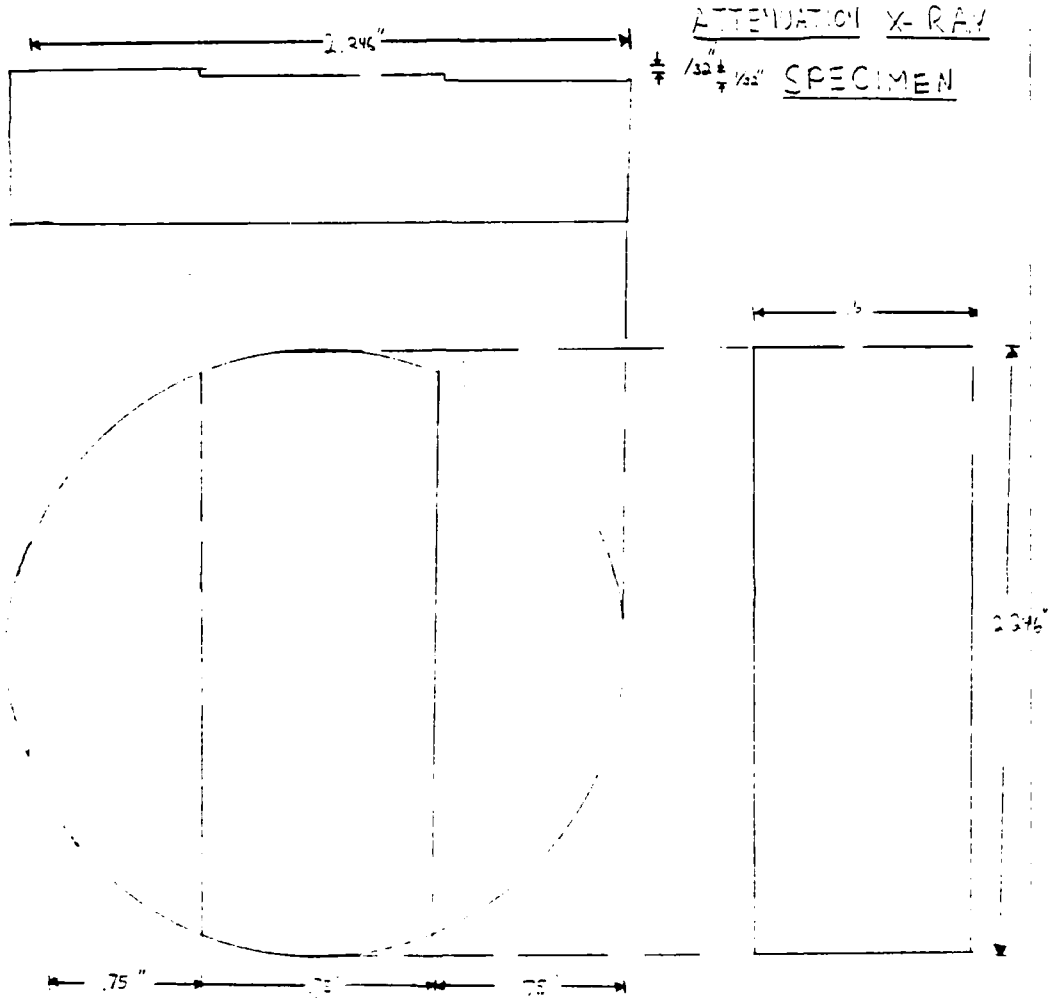

MATERIALS: ALUMINUM; TITANIUM; MILD STEEL

Figure 3 - Stepped specimen design for attenuation studies

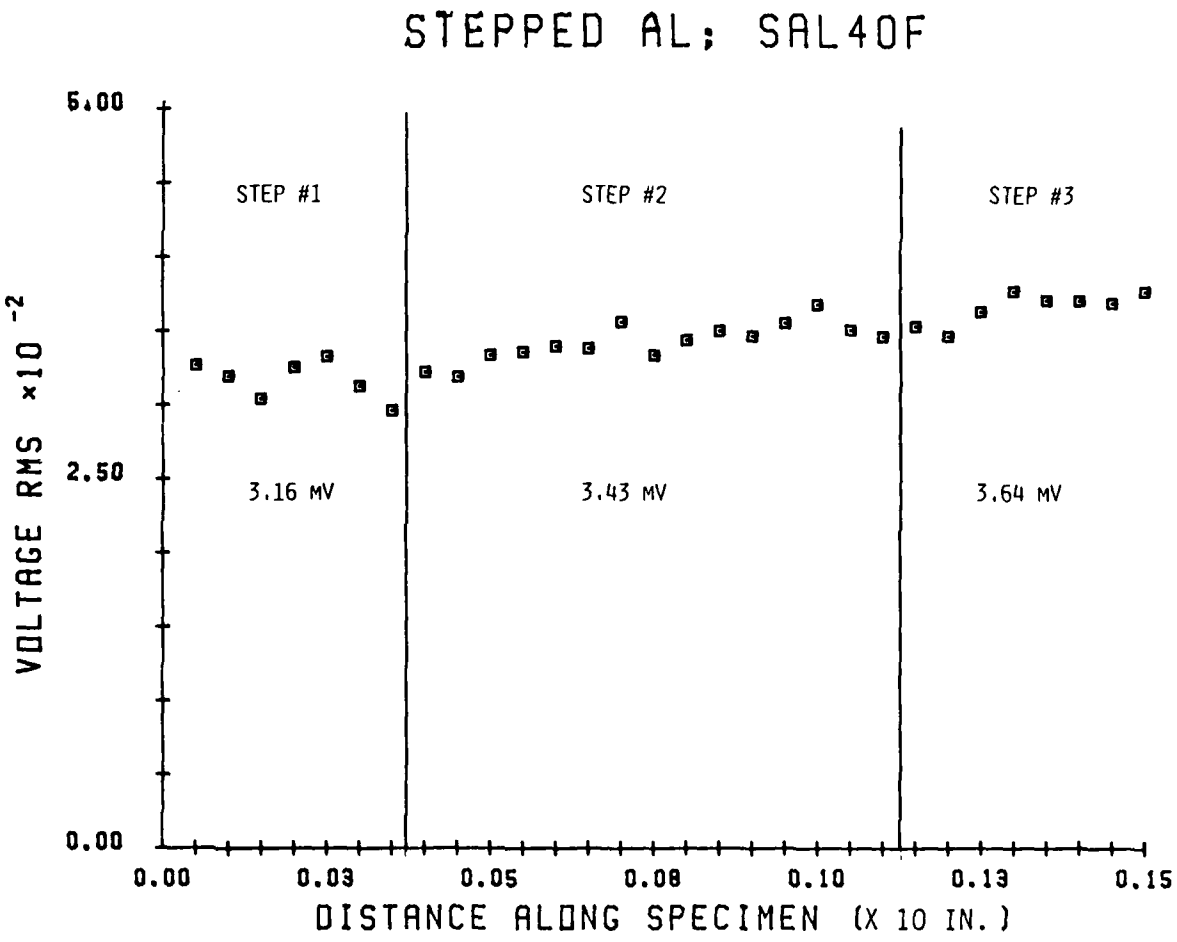

Figure 4 - rms Signal Amplitude; Stepped Aluminum Specimen

Figures 5(a) - (c) -

Broad-beam generated
x-ray/acoustic signals.

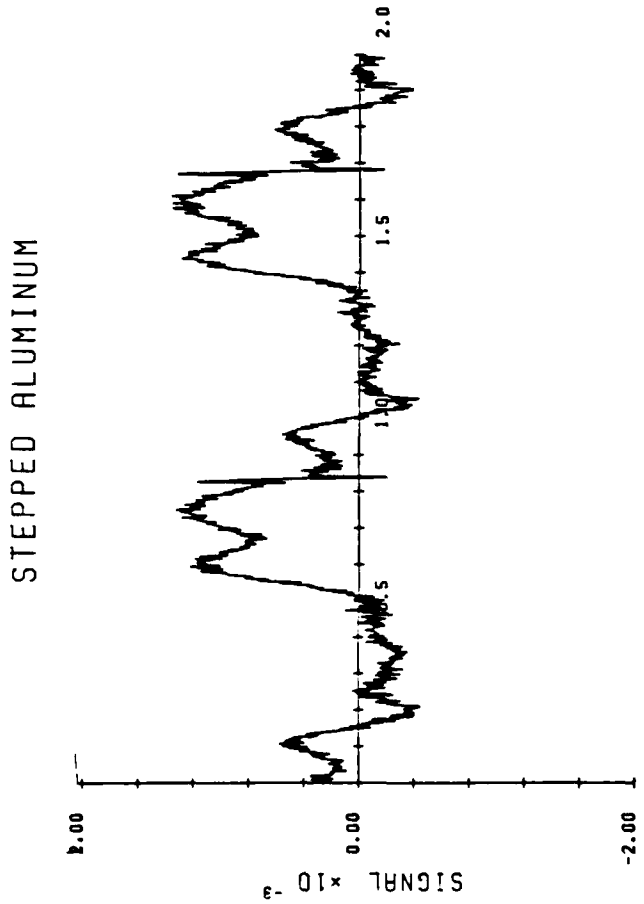

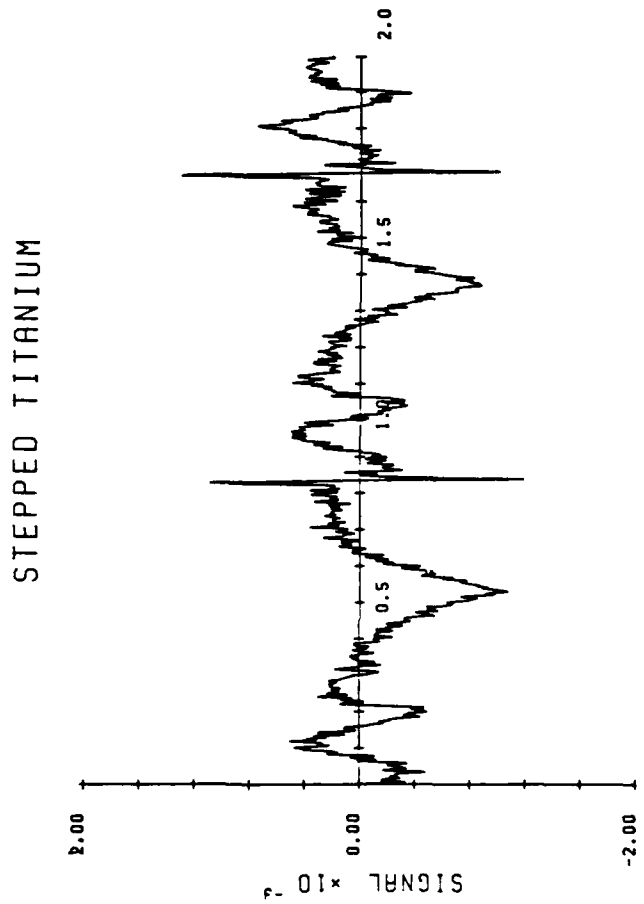

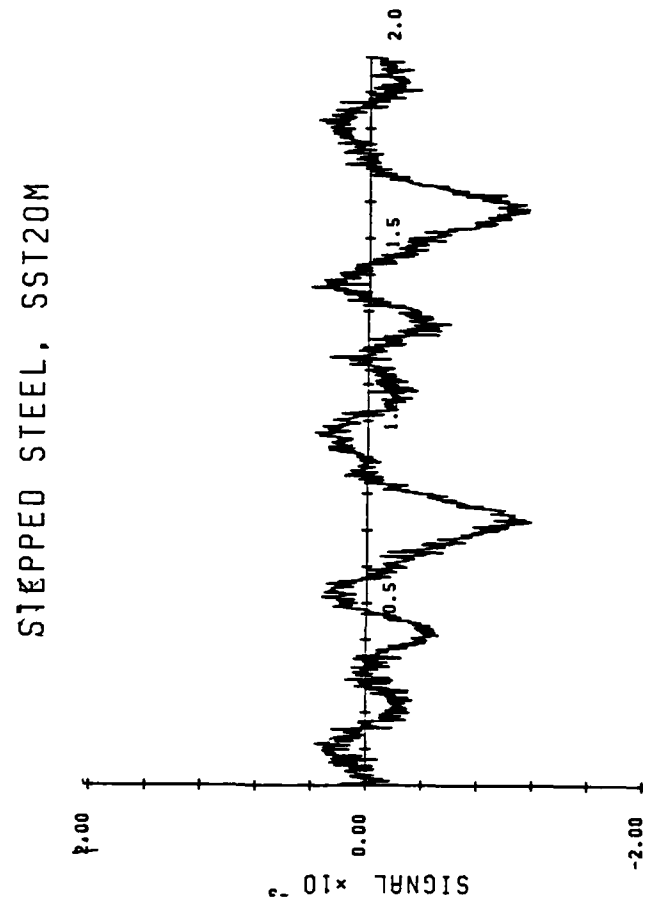

1000Å METAL FILMS ON FUSED SILICA

Figure 6

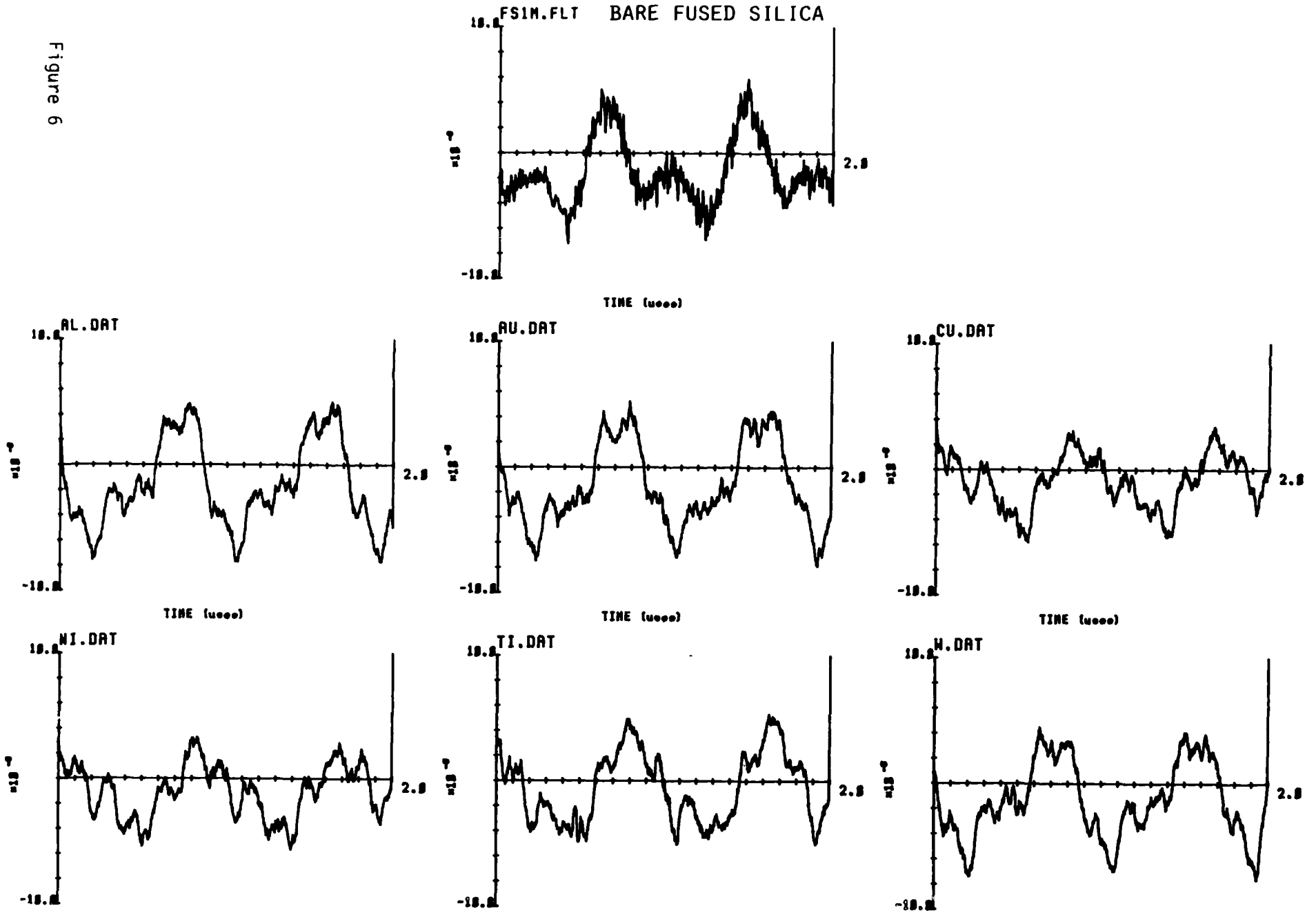

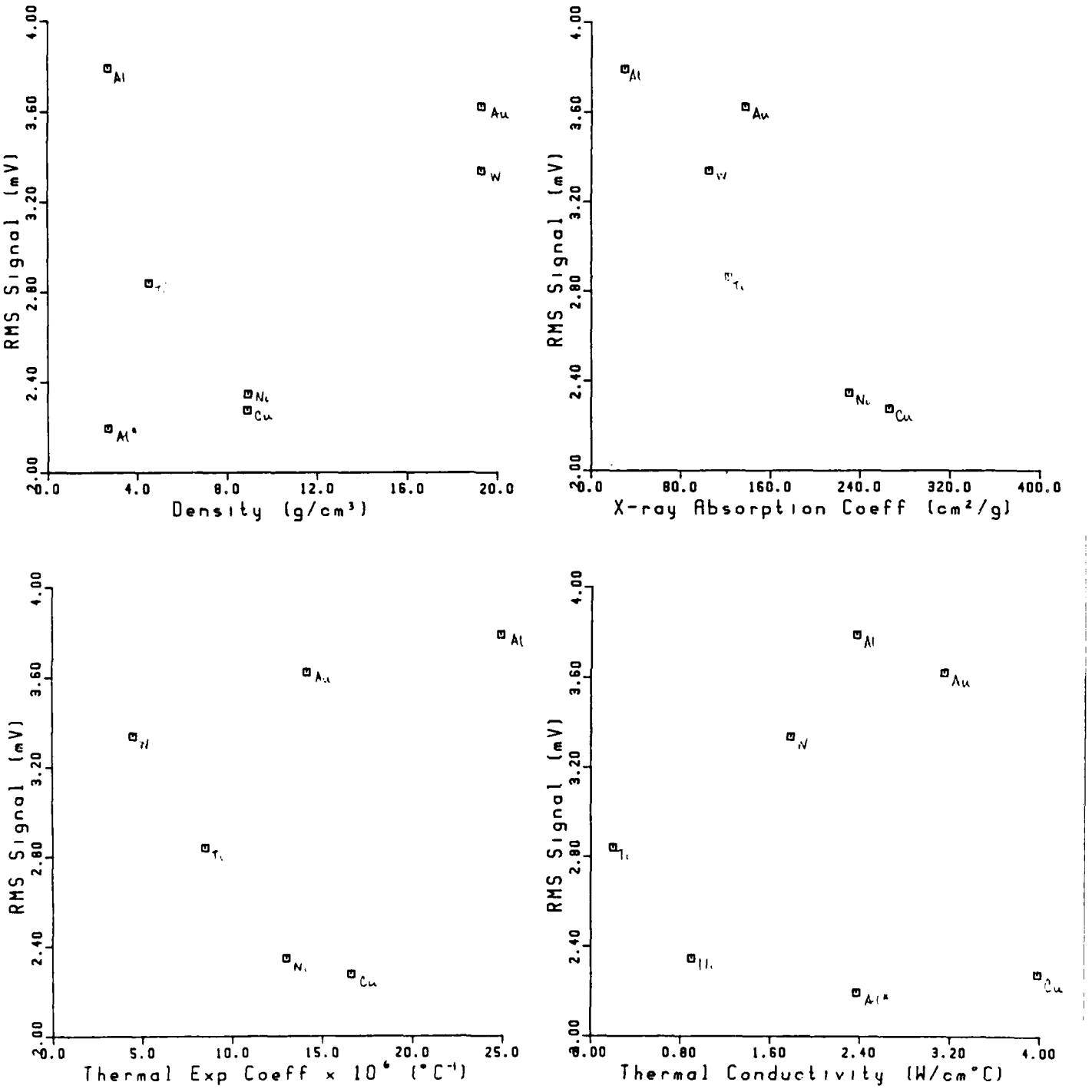

Figures 7 (a) - (d) - Composite Plots; X-ray/Acoustic Signals from Thin Metal Films on Fused Silica.

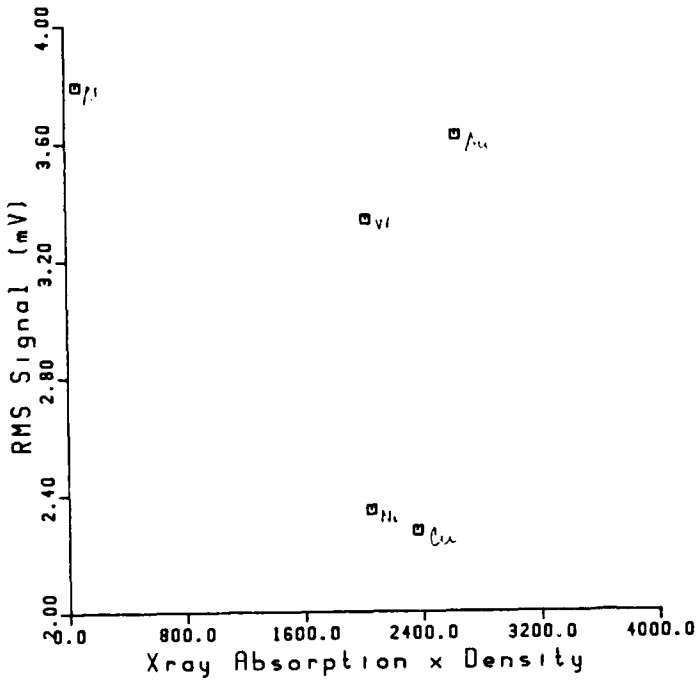

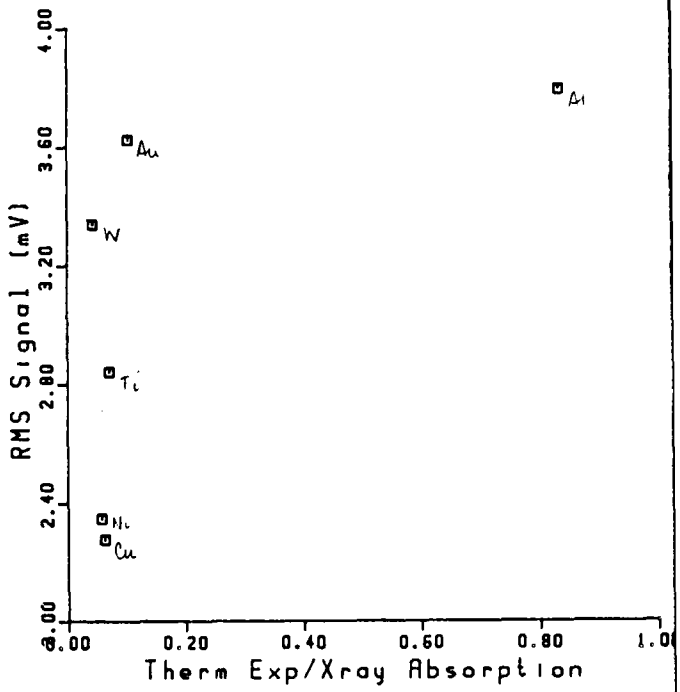

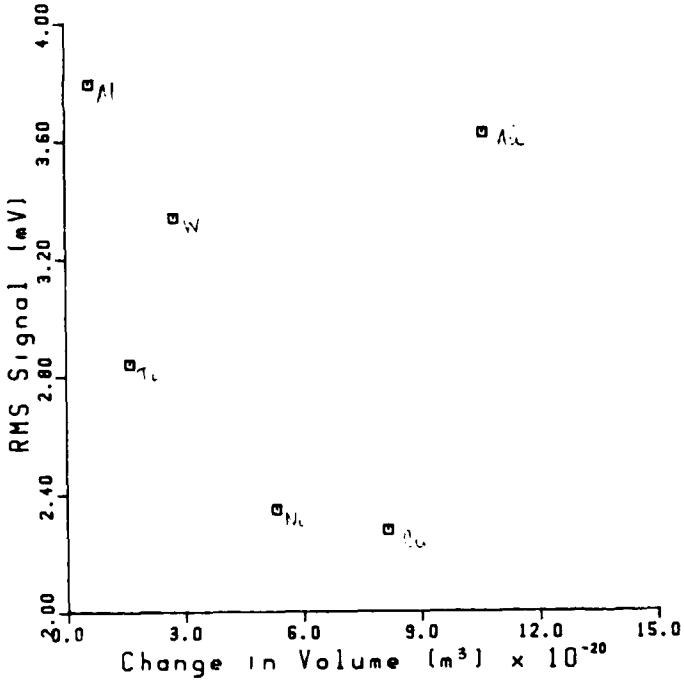

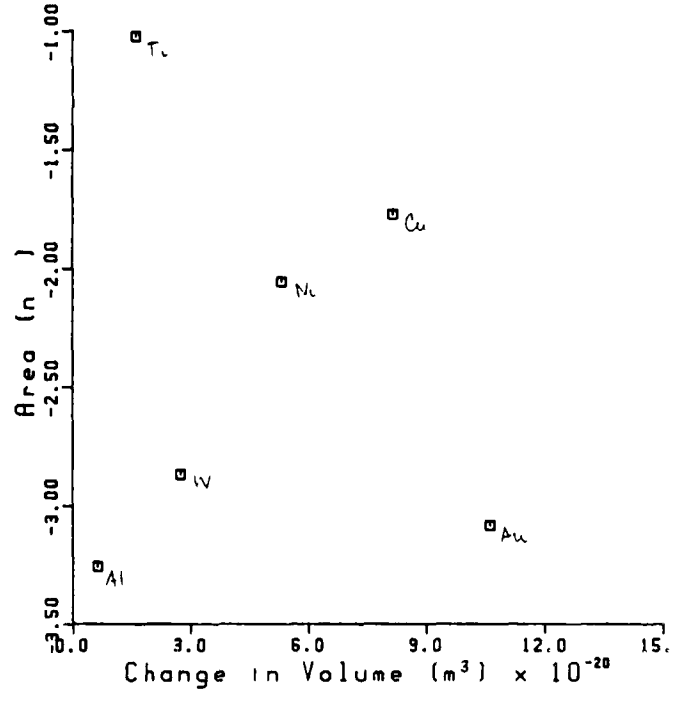

Figures 7 (e) - (h) - Composite Plots; X-ray/Acoustic Signals from Thin Metal Films on Fused Silica.

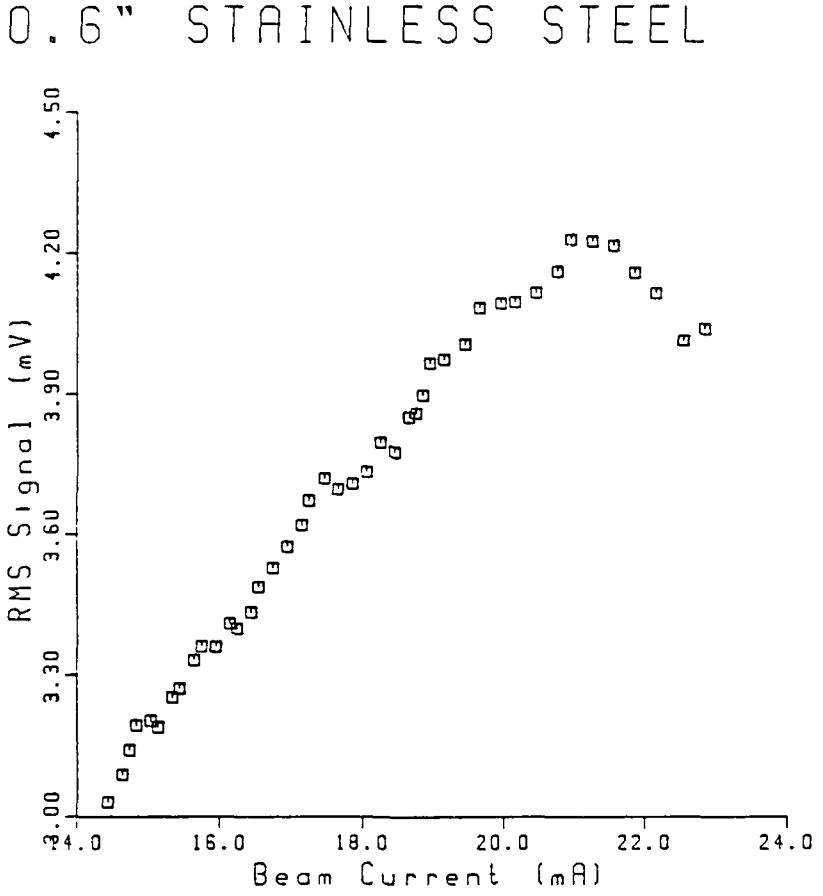

Figure 8 - rms Signal, Beam Current Dependence in Stainless Steel

STAINLESS STEEL – File: SS97VR.P4

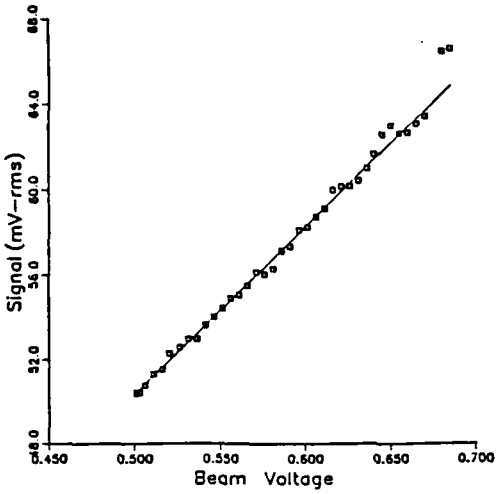

Slope: 79.16

Y-Intercept: 10.75

STAINLESS STEEL – File: SS3VR.P4

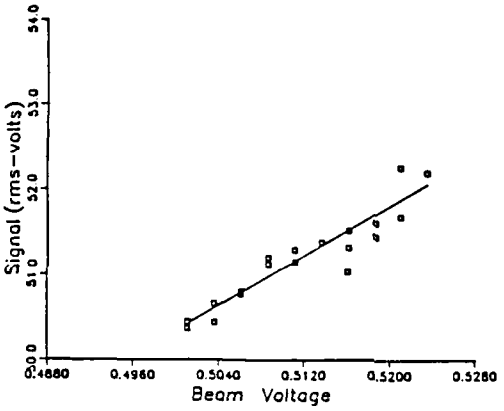

STAINLESS STEEL – File: SS20VR.P4

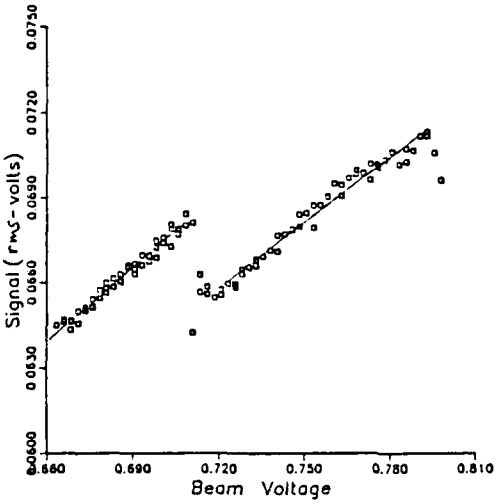

Figure 9 - Signal/Beam Current Dependence in Stainless Steel

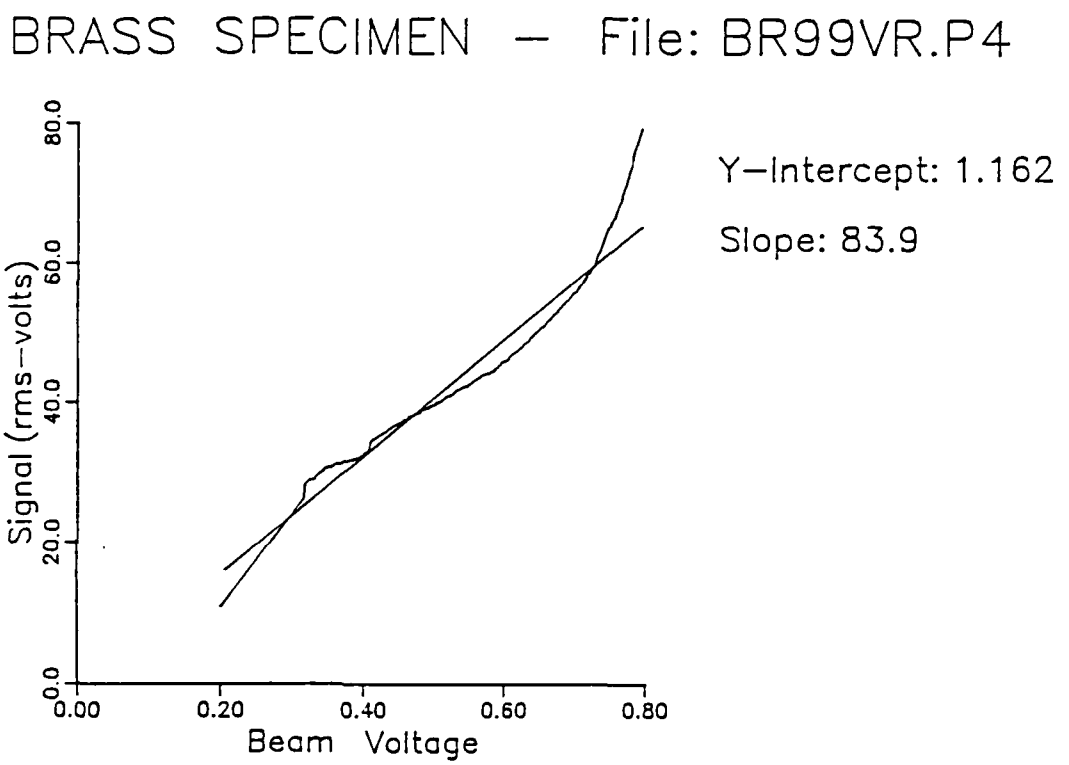

Figure 10 - Signal/Beam Current Dependence in Brass

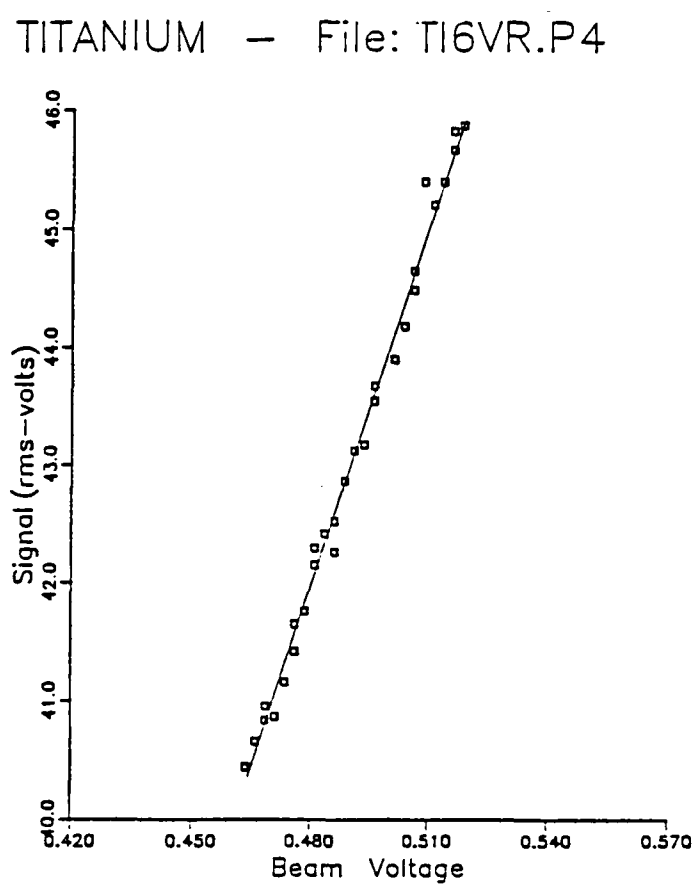

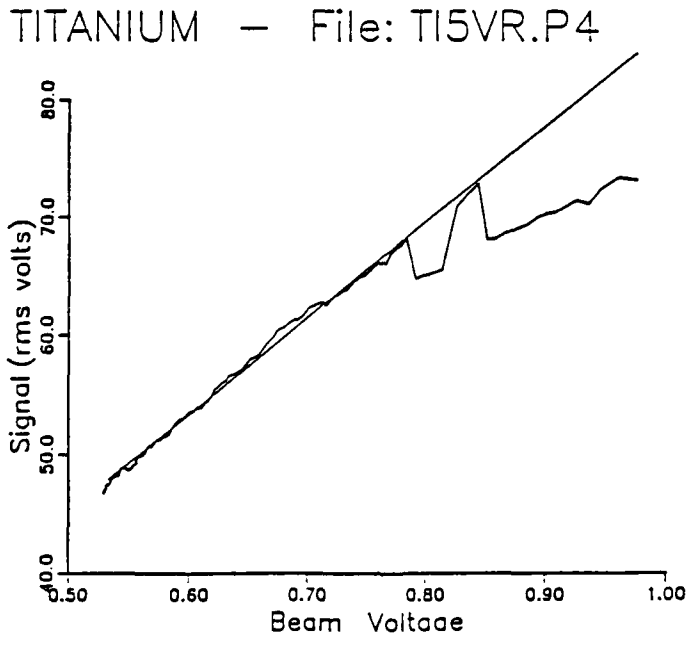

Figure 11 - Signal/Beam Current Dependence in Titanium

COPPER – File: CU99VR.P4

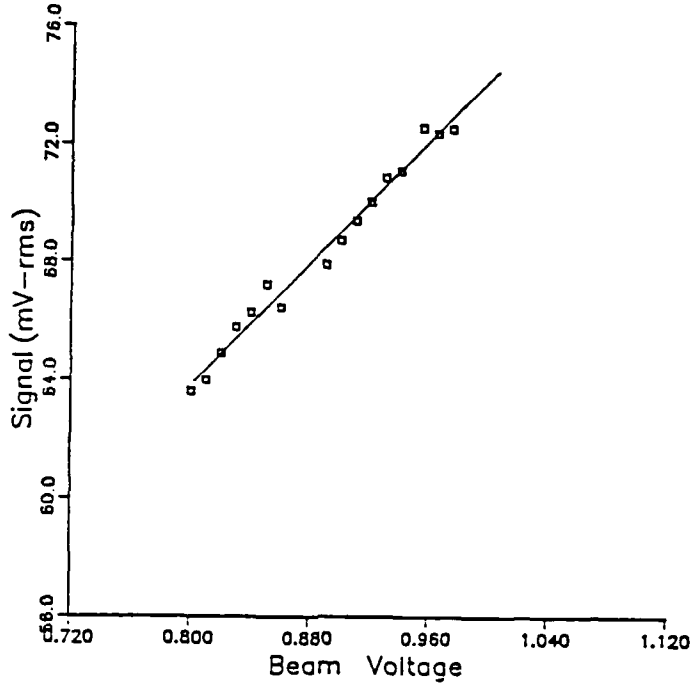

Slope: 51.80

Y–Intercept: 22.39

MILD STEEL – File: MS99VR.P4

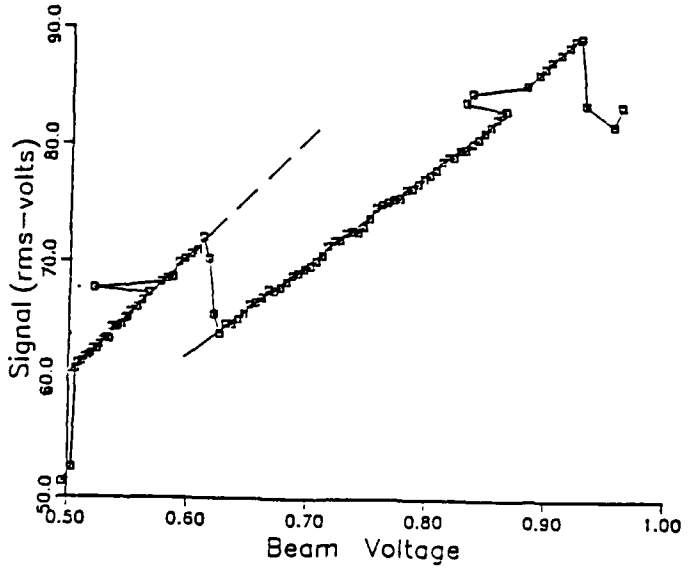

Slope: 77.98

Y–Intercept: 15.32

Slope: 103.2

Y–Intercept: 8.758

Figure 12 (a) - (b) - Signal/Beam Dependence in Copper and Mild Steel

X-RAY/ACOUSTIC APERTURE EFFECT

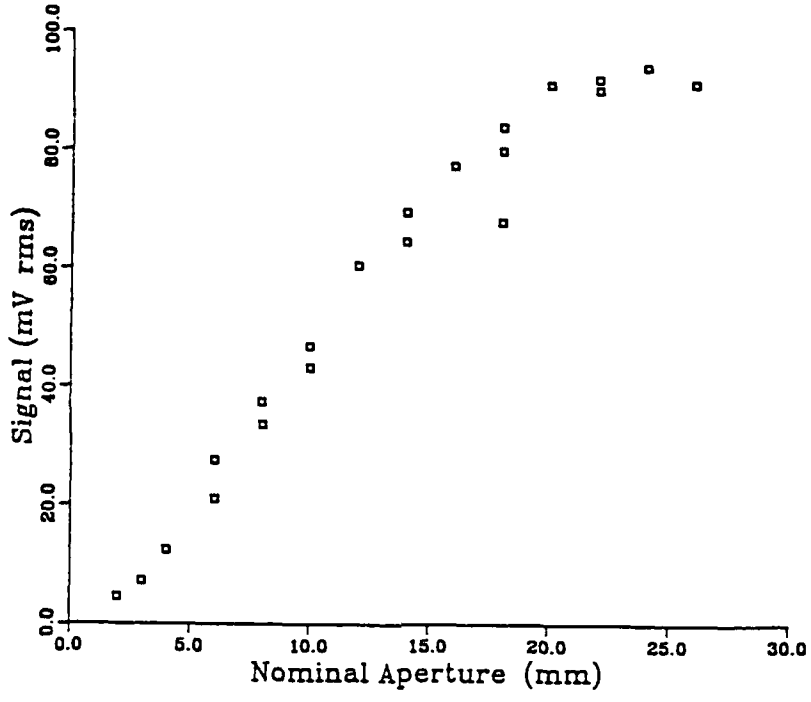

Figure 13(a) - rms Signal/Beam Aperture Dependence in Brass

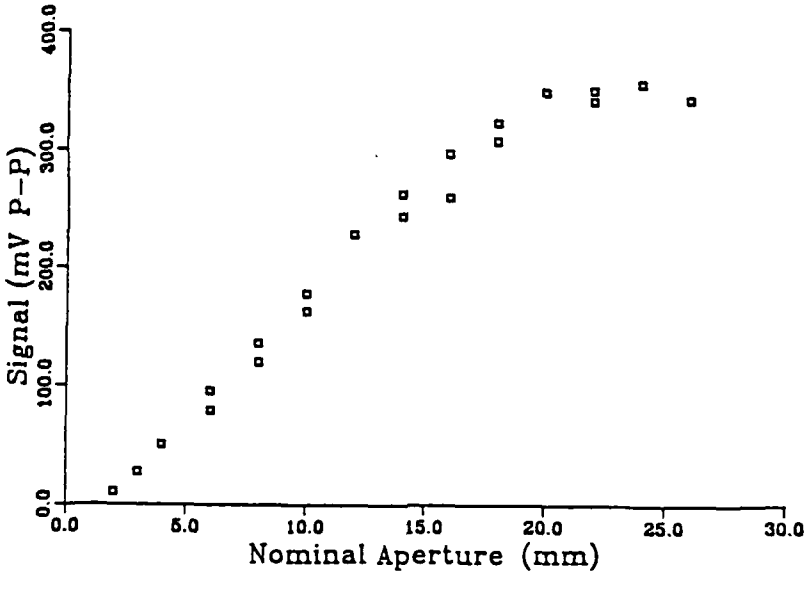

Figure 13(b) - P-P Signal/Beam Aperture Dependence in Brass

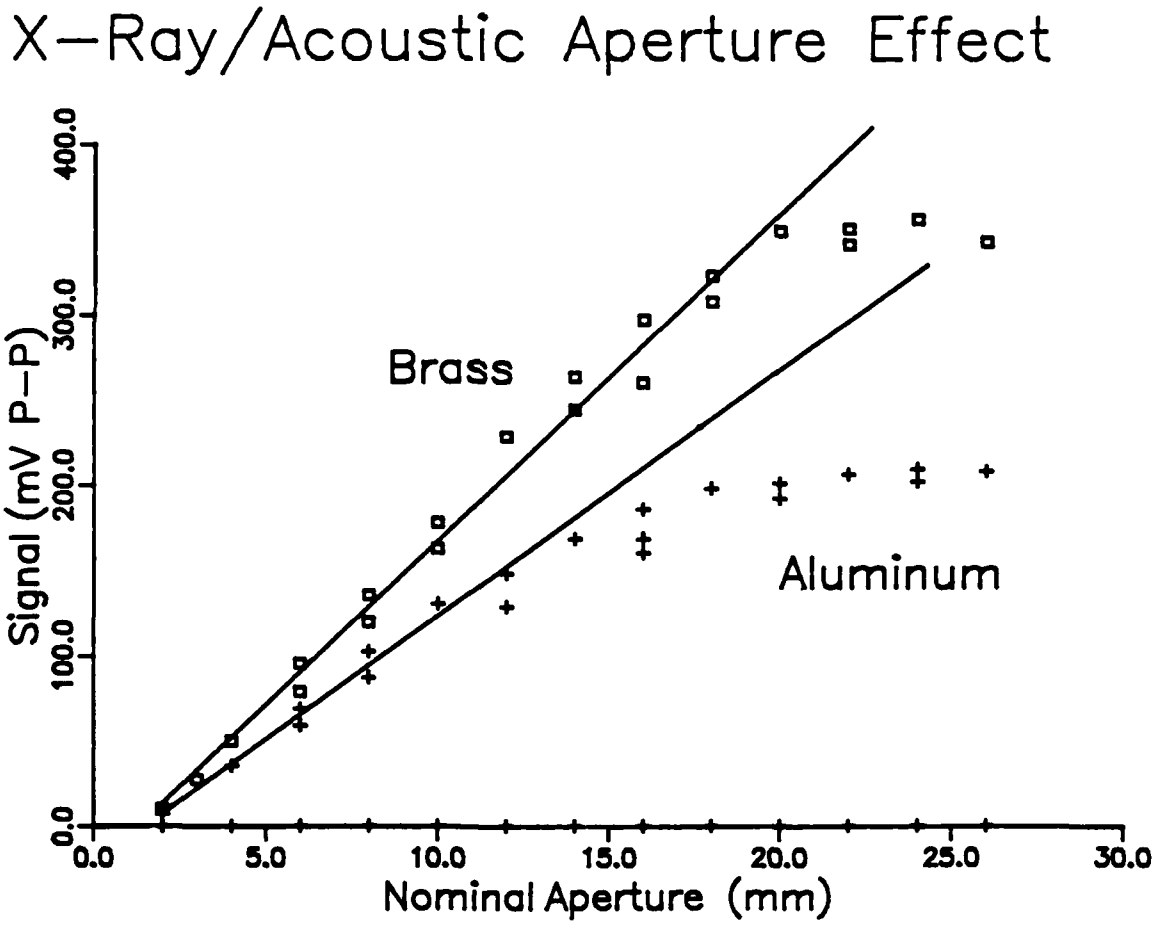

Figure 14 - P-P Signal/Beam Aperture Effect in Brass, Aluminum

ALUMINUM – Aperture Effect (4, 24 mm)

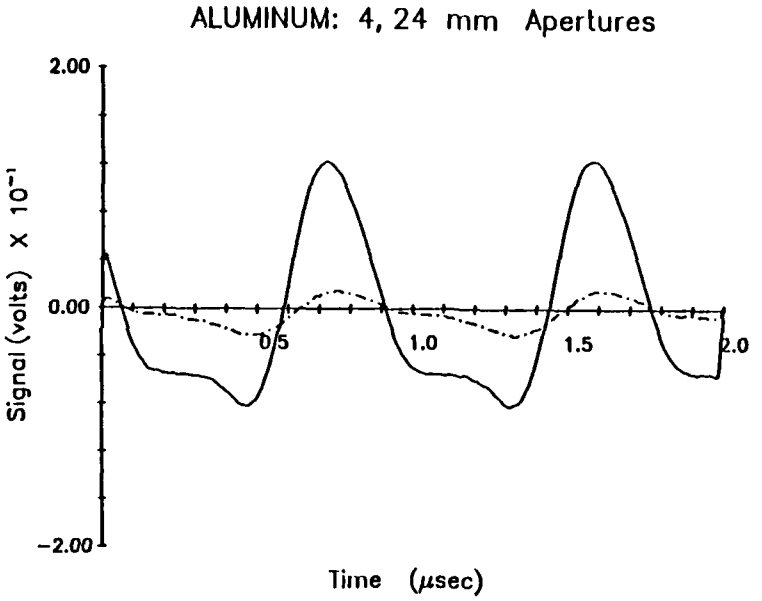

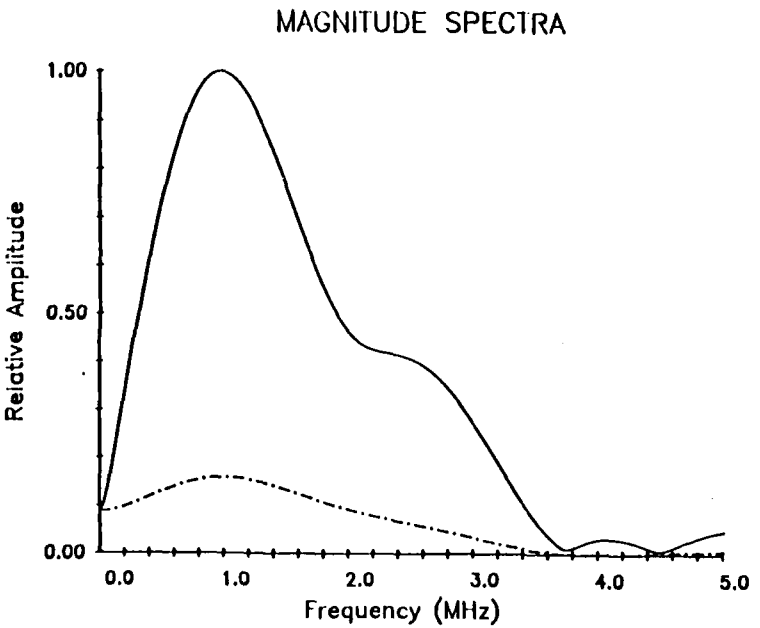

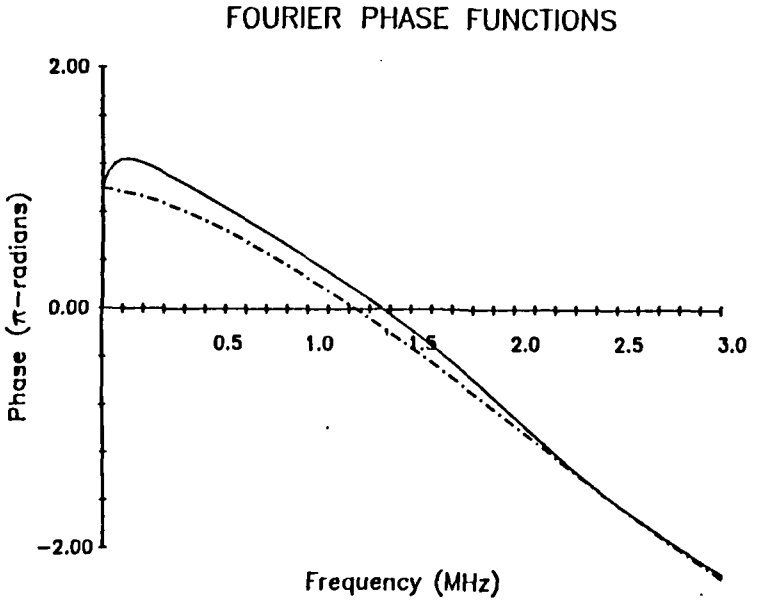

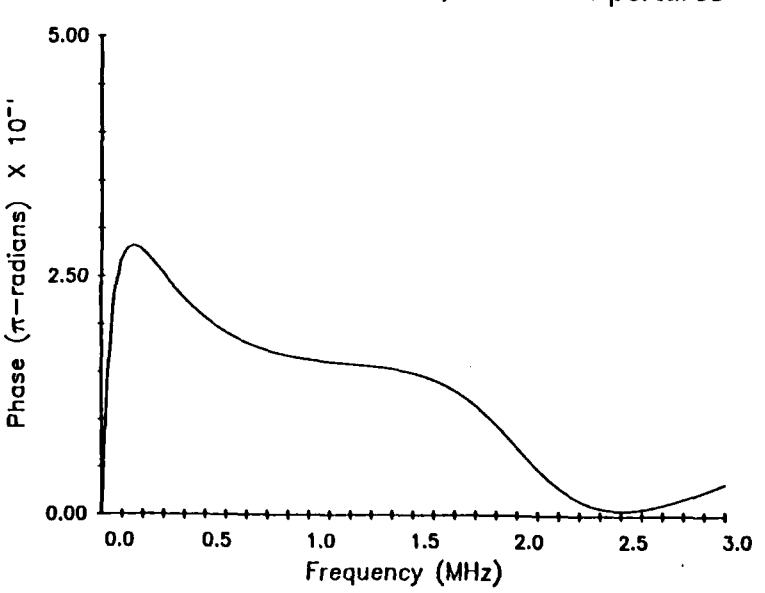

Figures 15 (a) - (d)

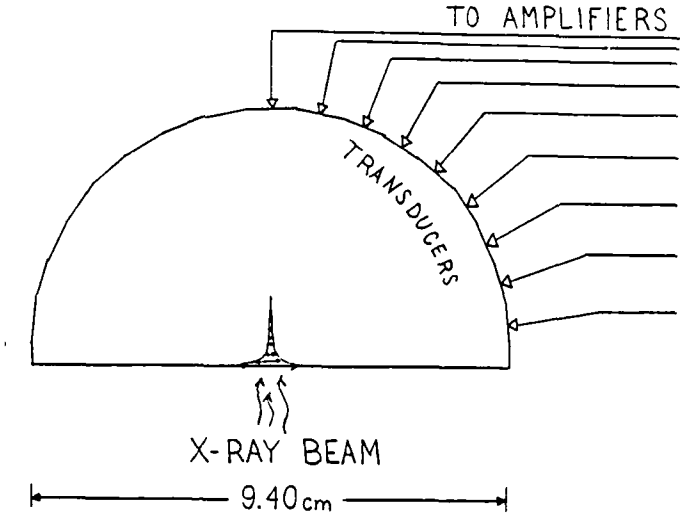

Figure 16 - Specimen and Test Configuration for X-ray/Acoustic Directivity Tests.

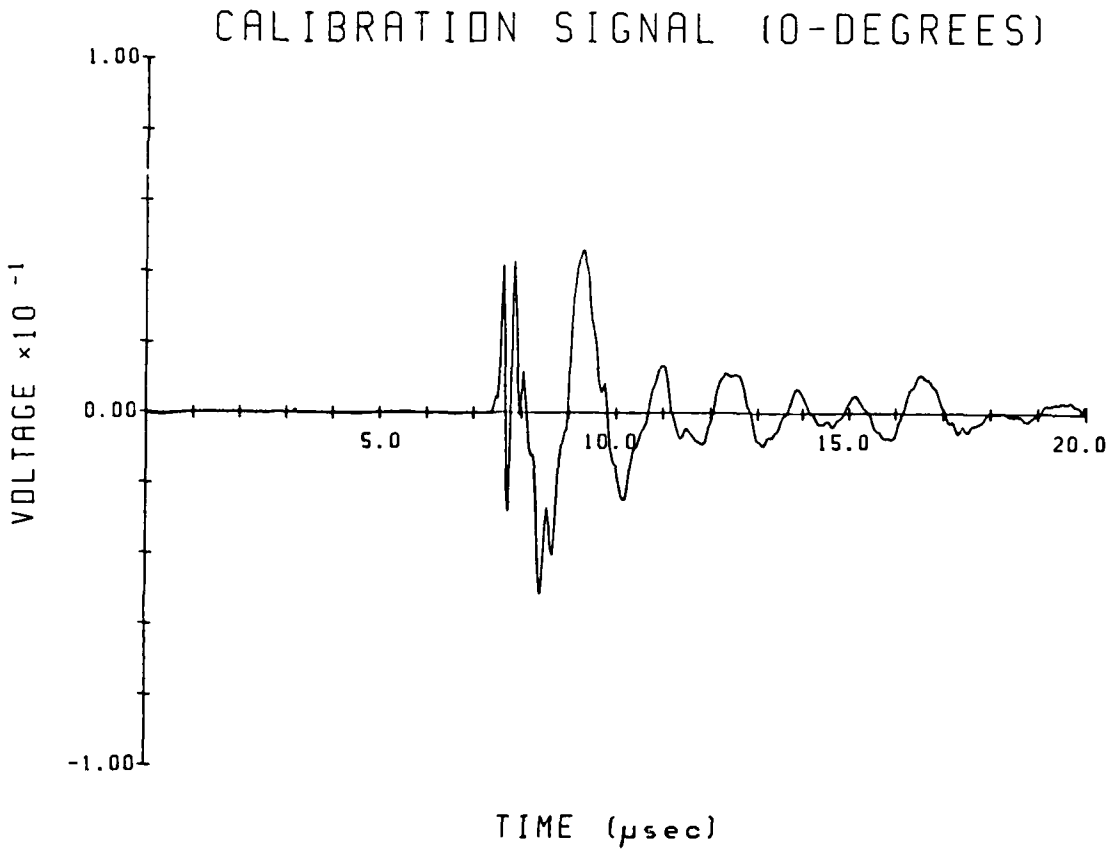

Figure 17 (a) - 0° Calibration Signal for X-ray Acoustic Directivity Tests.

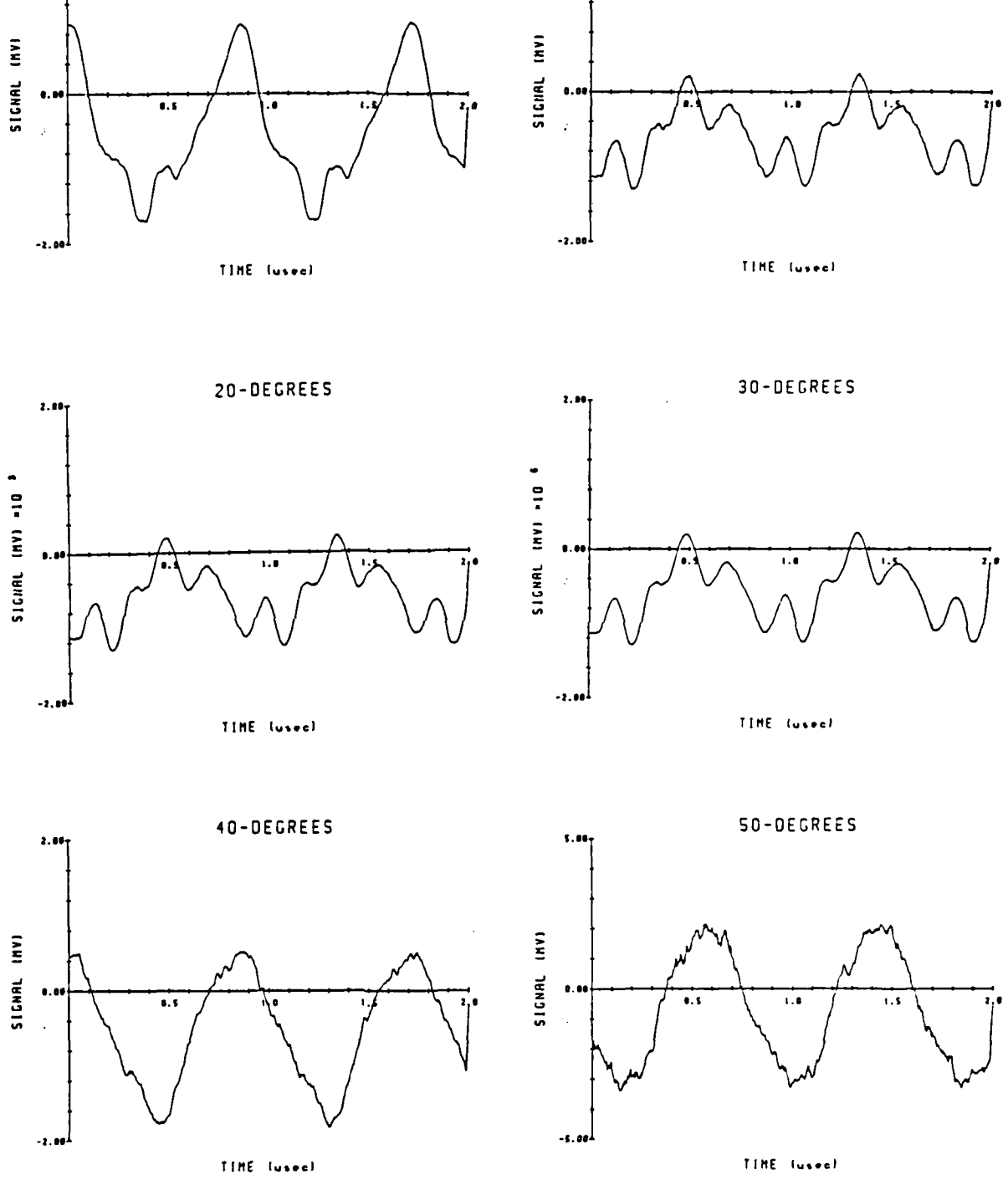

Figures 17 (b) - (g) - Determination of X-ray/Acoustic Directivity

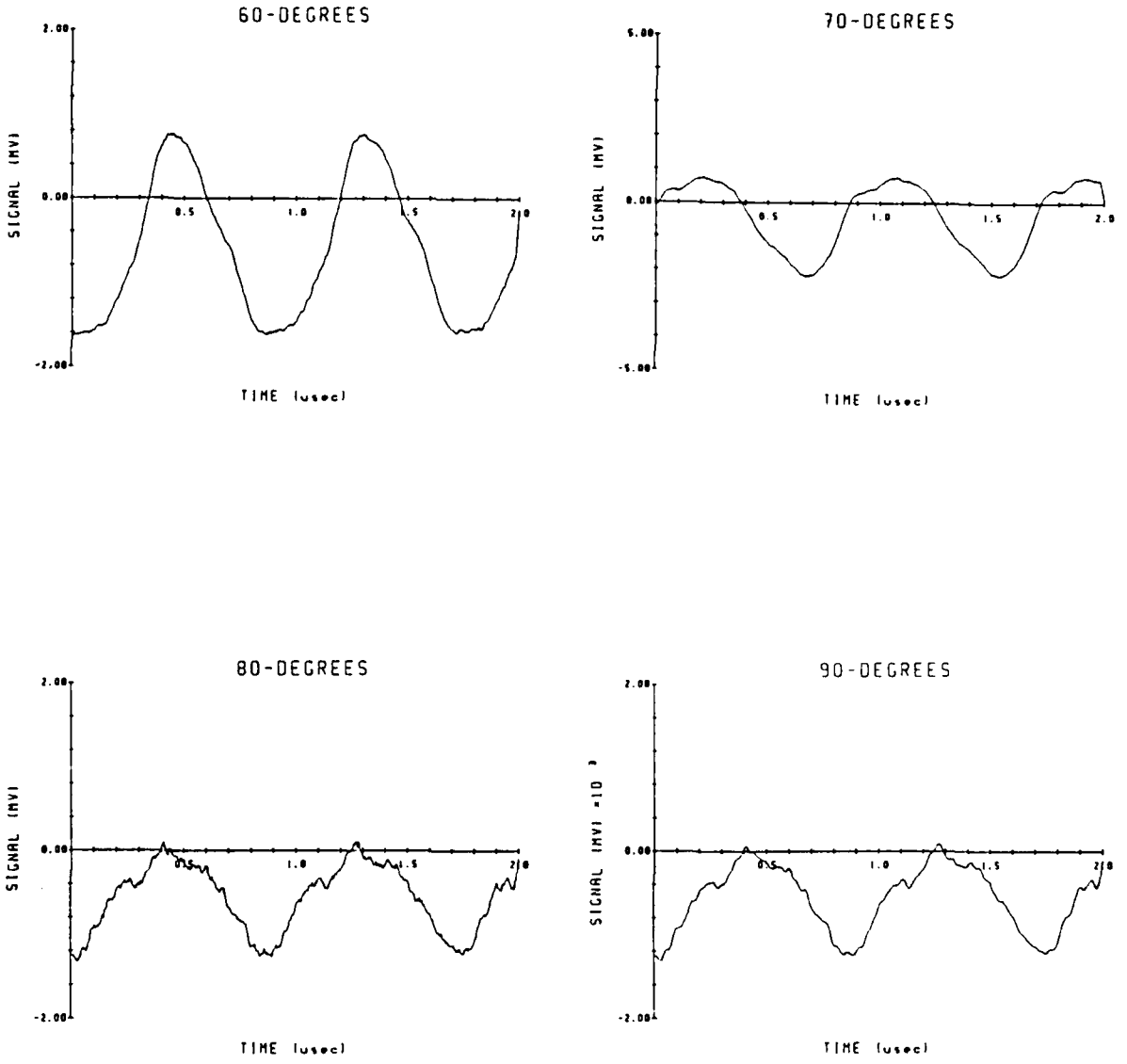

Figures 17 (h) - (k) - Determination of X-ray/Acoustic Directivity

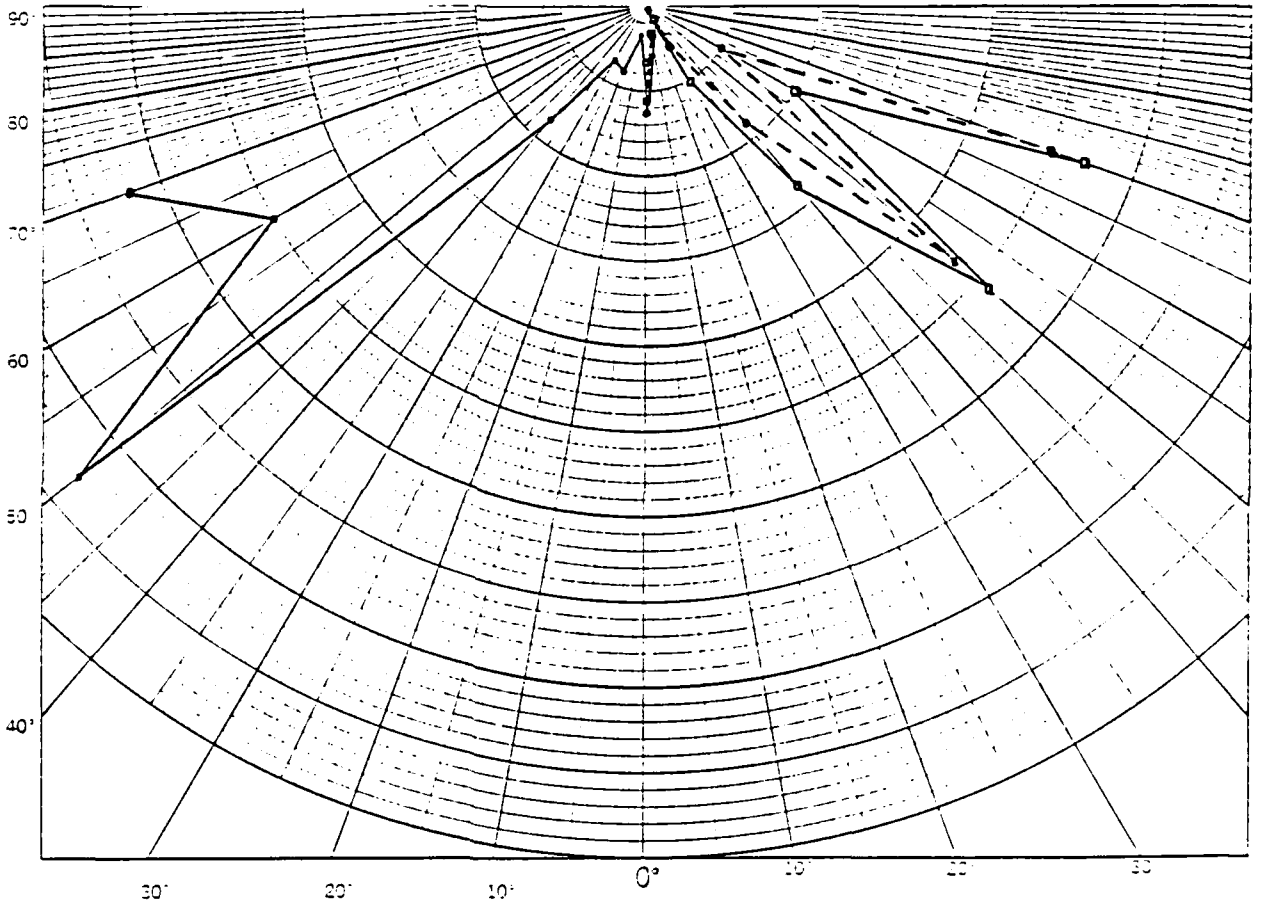

Figure 18 - Measured X-ray/Acoustic Signal Directivity;
On left: Wide X-ray Beam; On Right: Two tests, Narrow X-ray Beam.

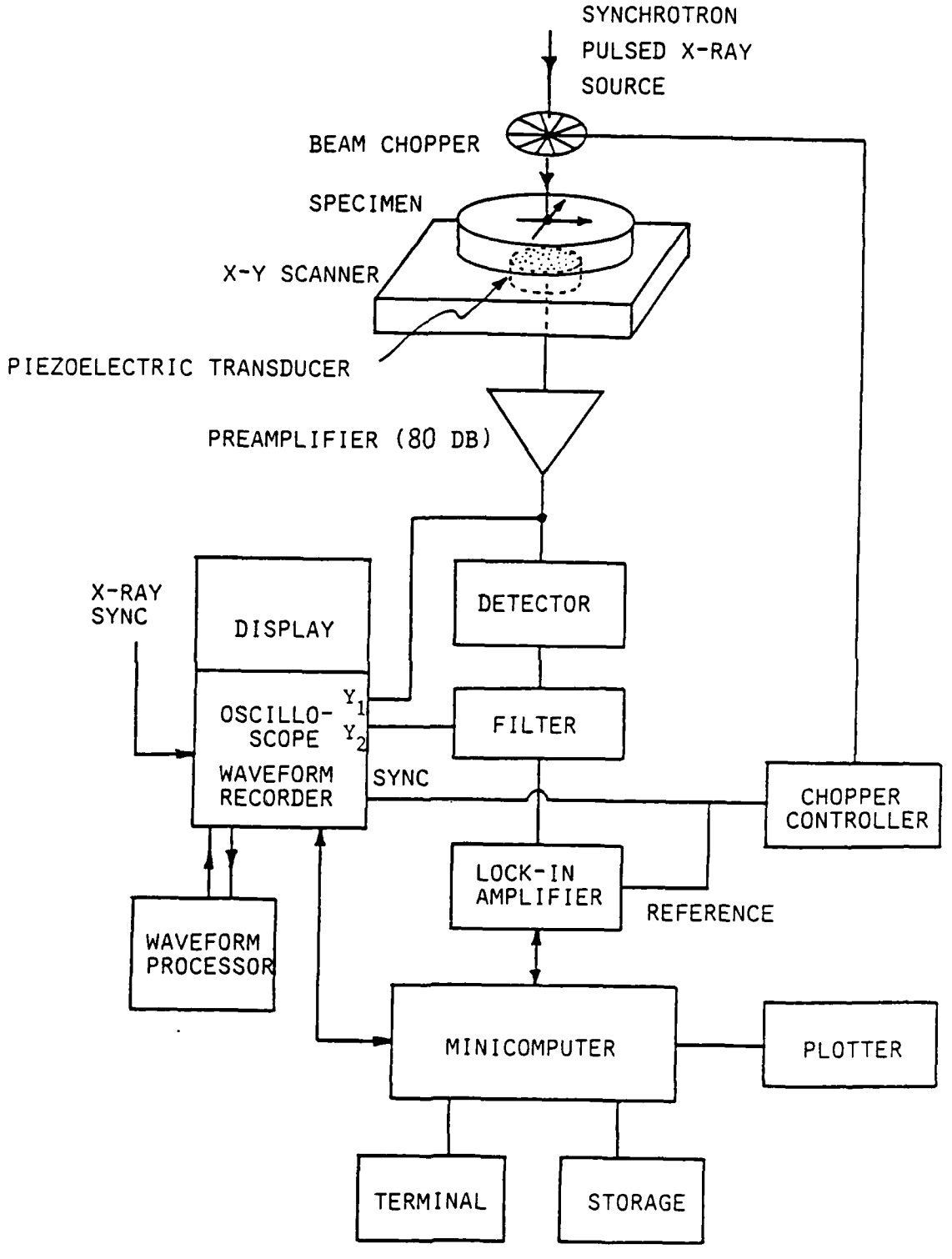

Figure 19 - X-ray/Acoustic Measurement System for Real-time Waveform Aquisition and Double Modulation Tests.

(a) X-RAY/ACOUSTIC SIGNAL (SLANT-HOLE, AL)

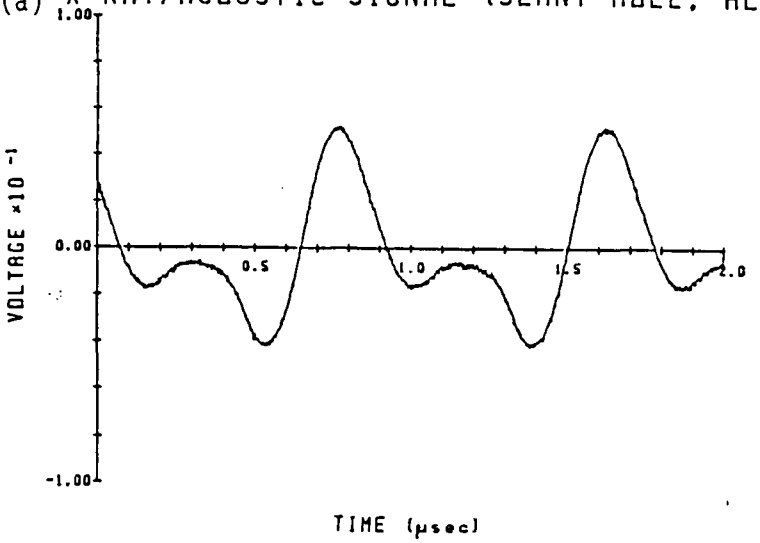

(b) CHOPPER-MODUL: X-RAY/ACOUSTIC SIGNAL

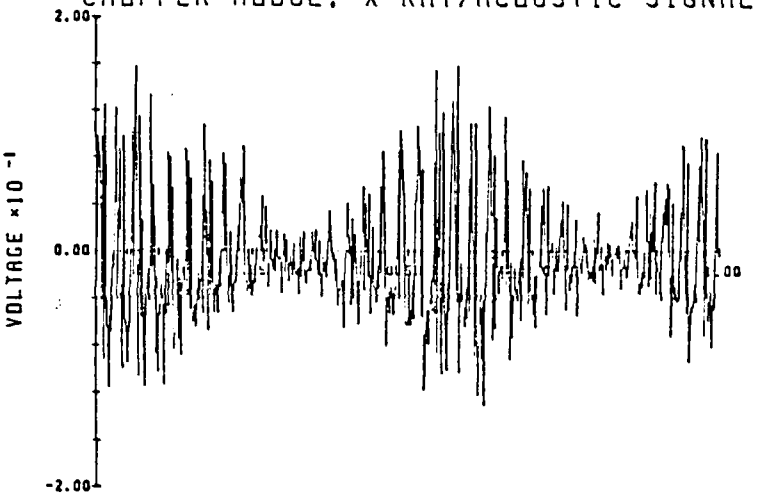

(c) 1.5 KHZ-MODULATED X-RAY/ACOUSTIC SIG

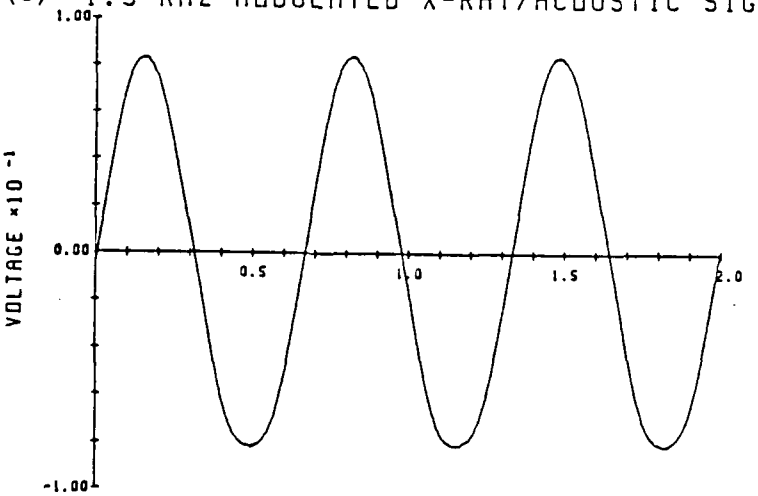

Figure 20

(a) X–RAY/ACOUSTIC SIGNAL MAGNITUDE

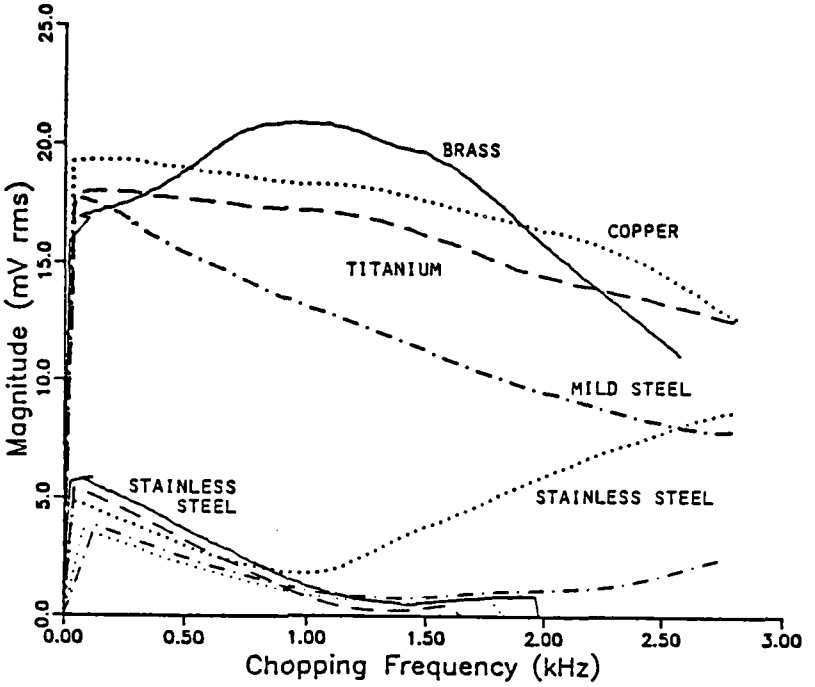

(b) X–RAY/ACOUSTIC SIGNAL PHASE

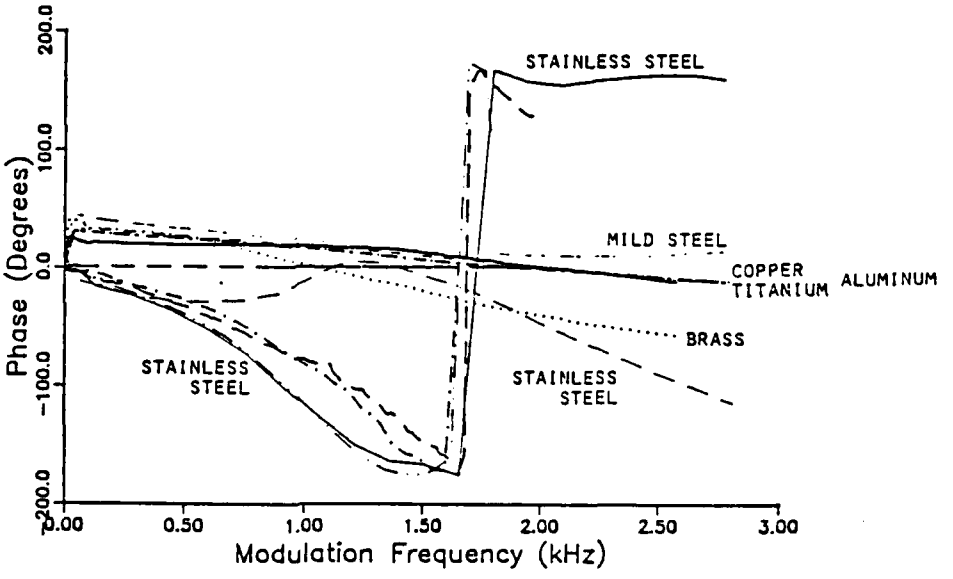

Figures 21 (a) - (b) - Results of Double Modulation Experiments

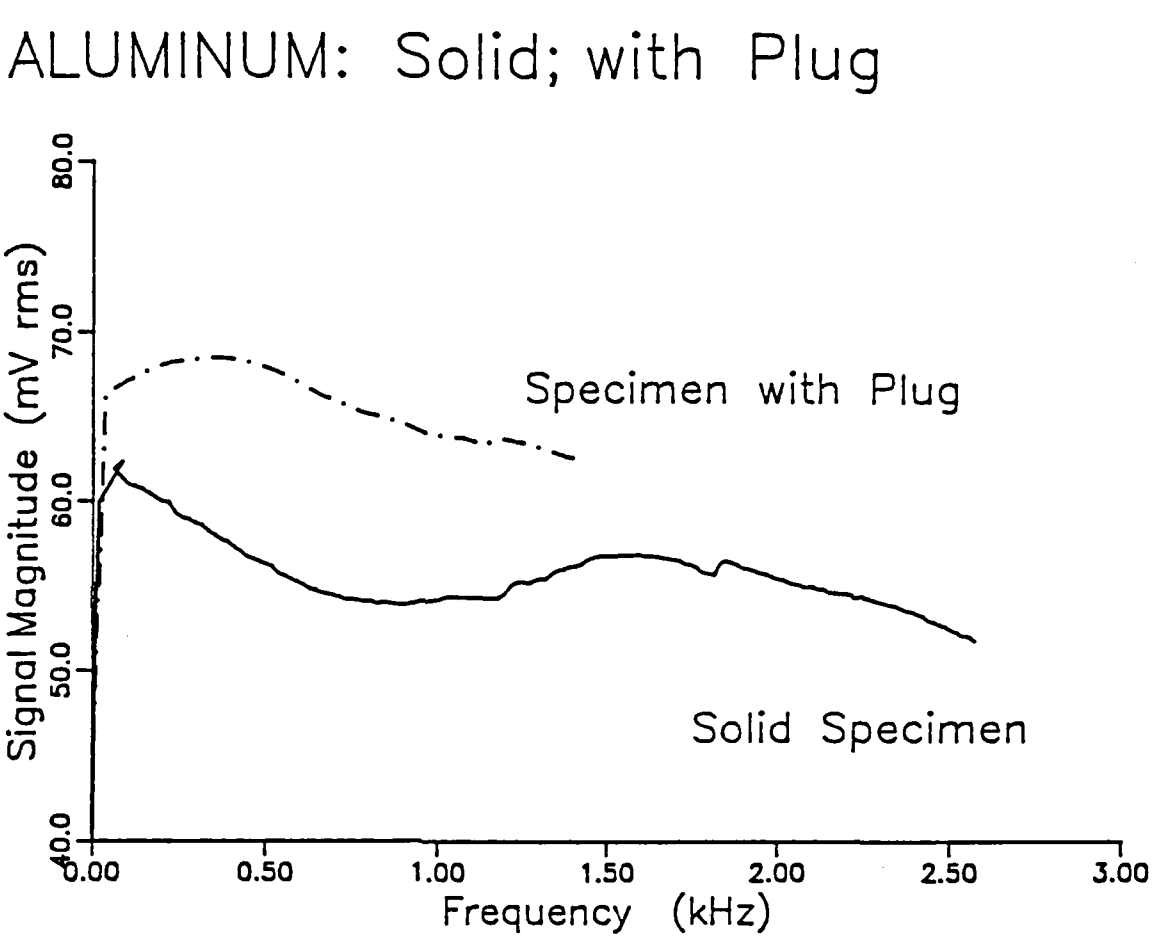

Figure 22 - Comparison of Solid Aluminum Specimen and one with Iron Plug inside. Double Modulation Measurement.

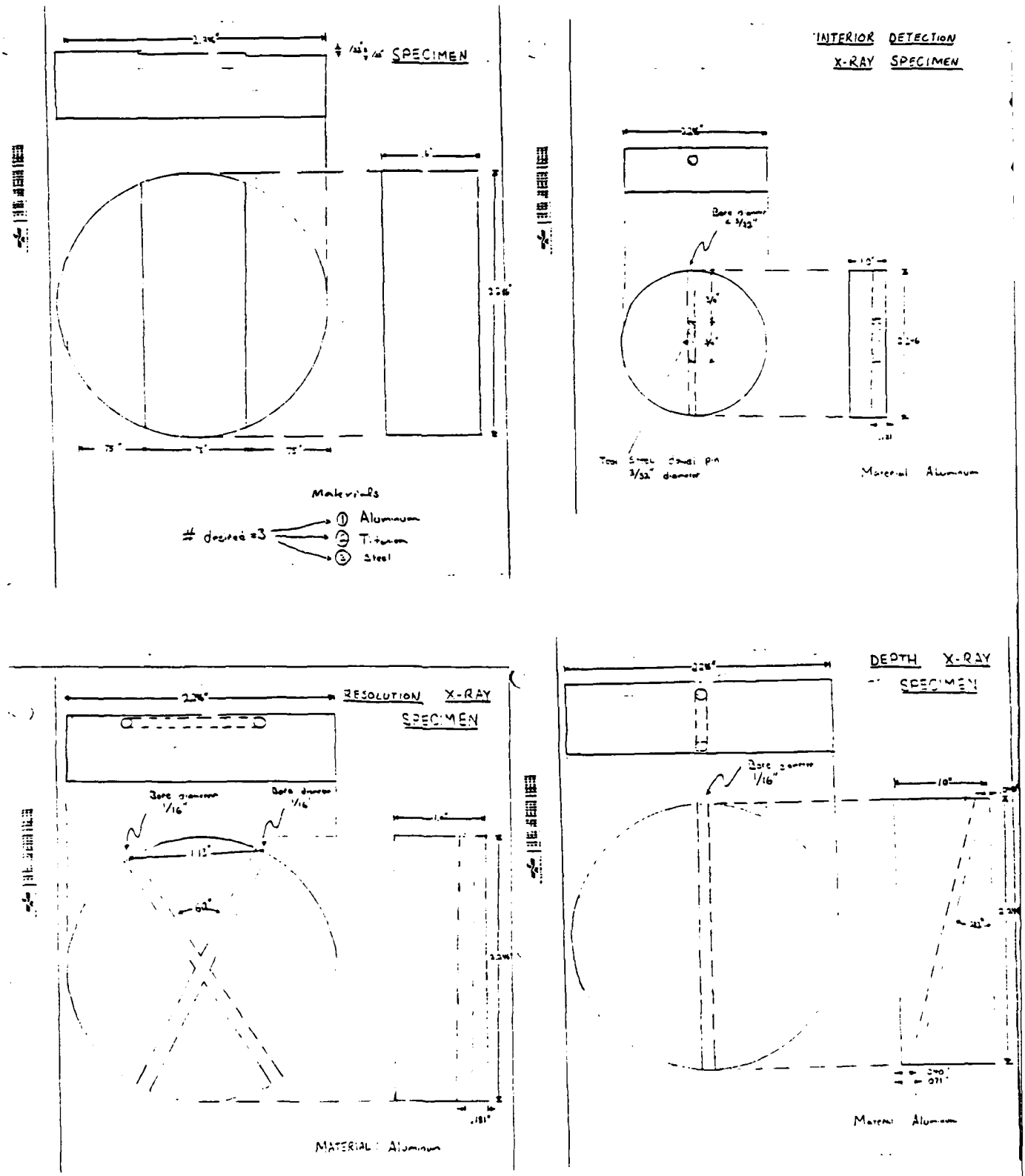

Figure 23 - Specimens tested in X-Y Scanning Measurements

(a) FILE: AL27.RMS ⊕ rms - Signal Amplitude

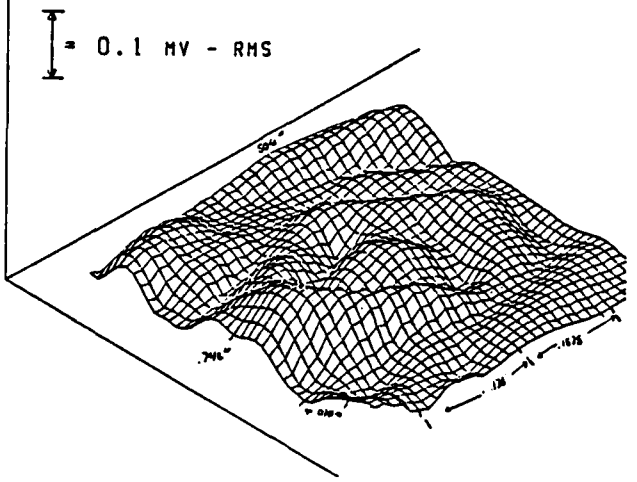

(b) FILE: AL27:RMS - Contour plot of the above

(c) FILE: AL27.DLY ○ - Signal delay (degrees)

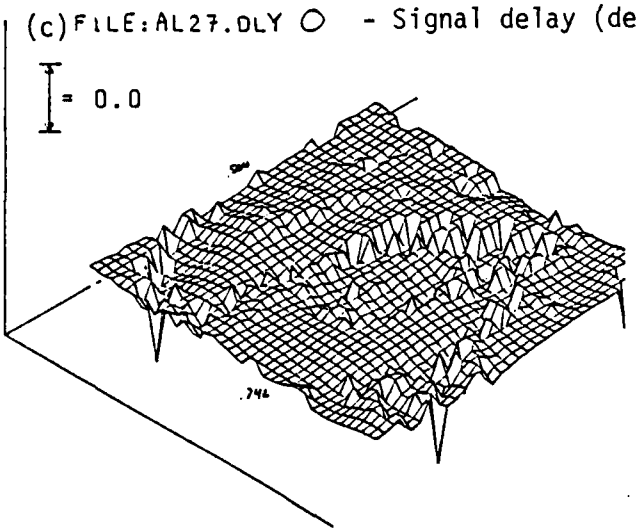

Figures 24 (a) - (c)

(a) FILE:AL23.M1 rms - Signal Amplitude

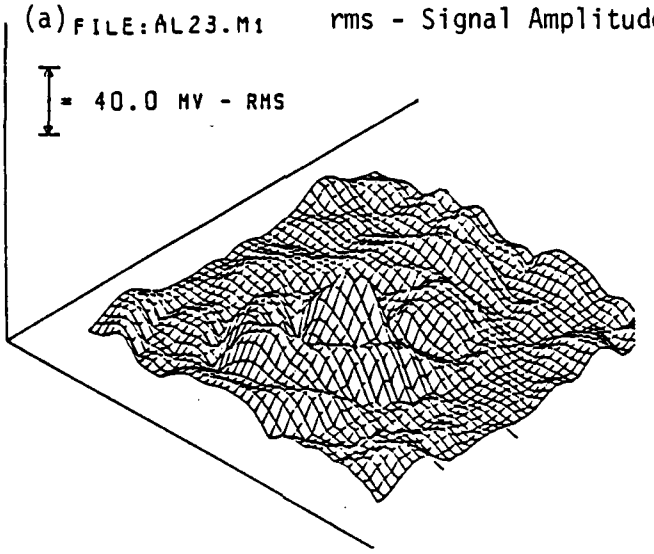

(b) FILE: AL23.M1 - Contour plot of the above

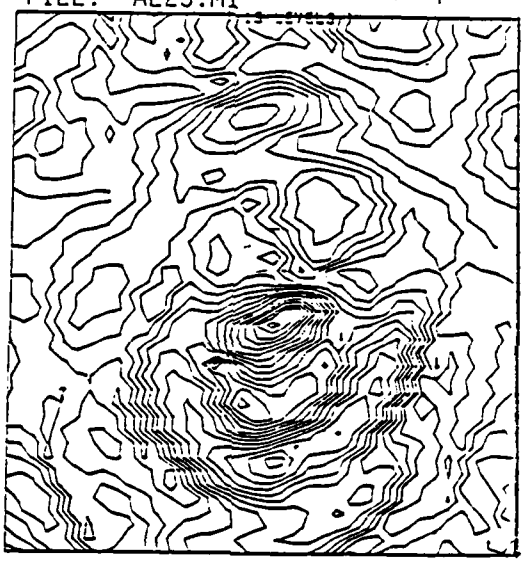

(c) FILE: AL23A.P1 - Signal delay (degrees)

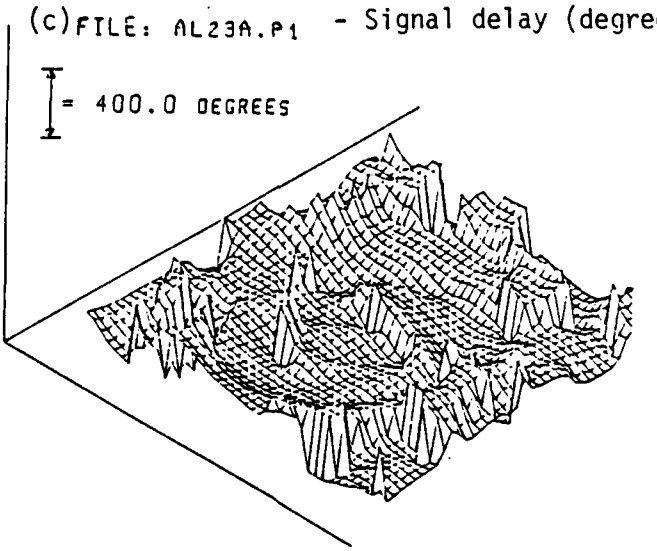

Figures 25 (a) - (c)

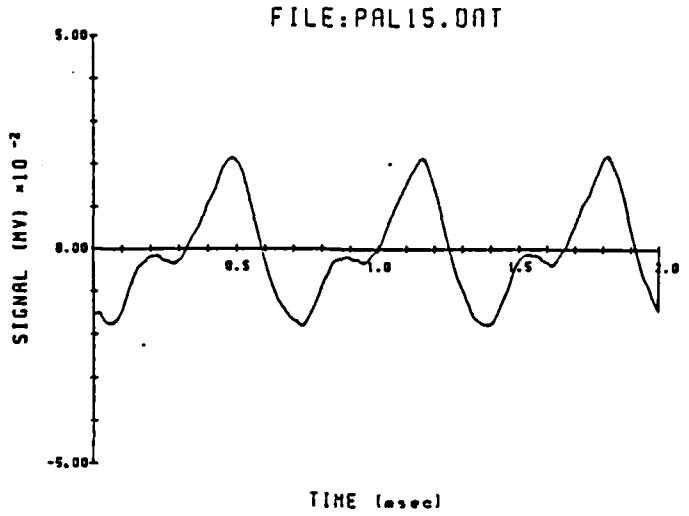

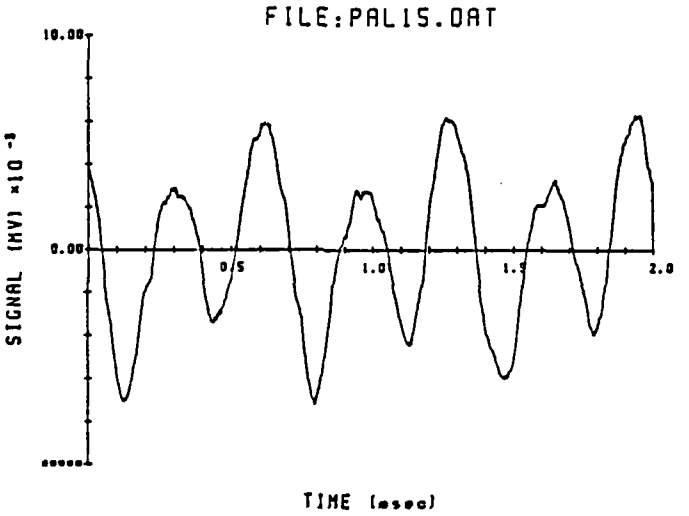

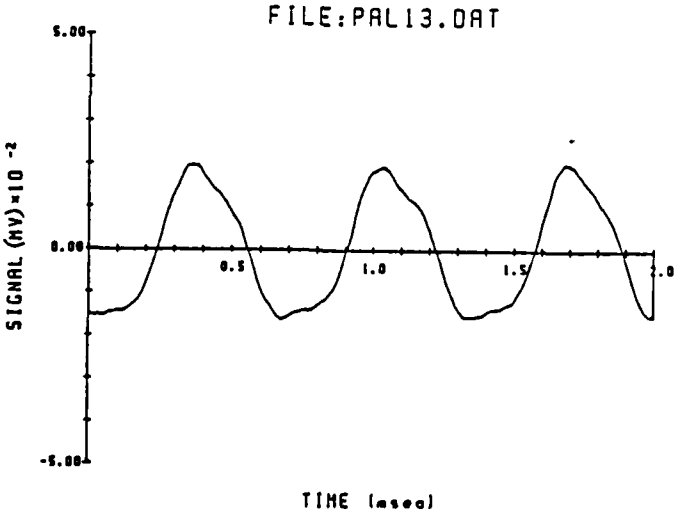

Figures 26 (a) - (c) - Waveforms measured at three points on a scan line

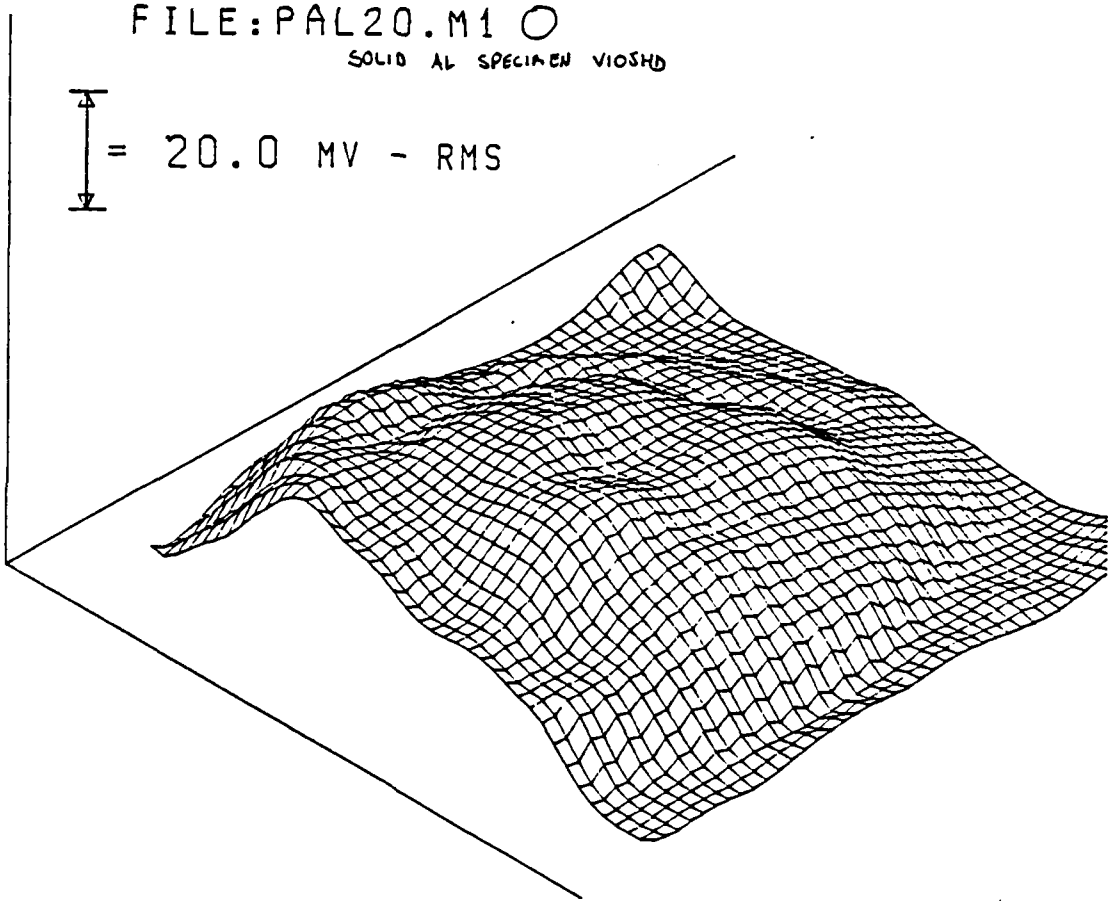

Figure 27 - rms Signal Amplitude determined with an 18.75 mm Diameter, 2.25 MHz Transducer in Aluminum.

(a) FILE: AL28.RMS O - rms - Signal Amplitude

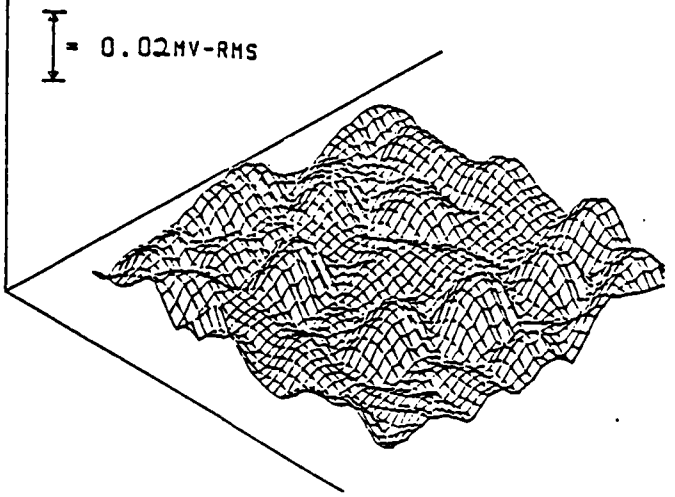

(b) FILE:AL28.DLY O - Signal Delay

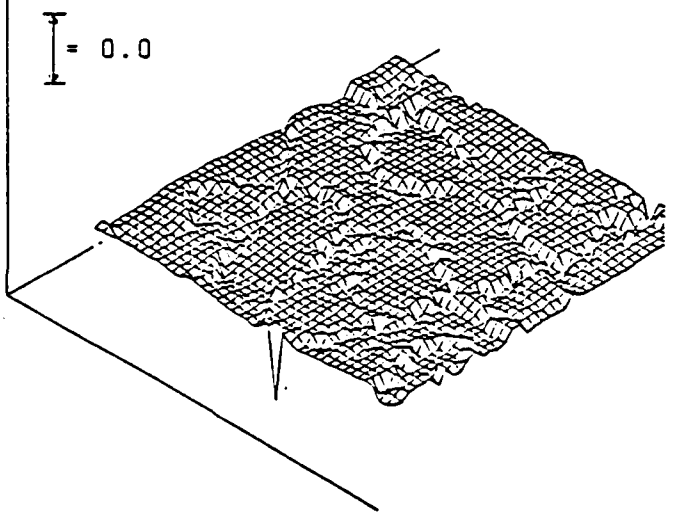

(c) AL28.RMS Contour Plot of (a)

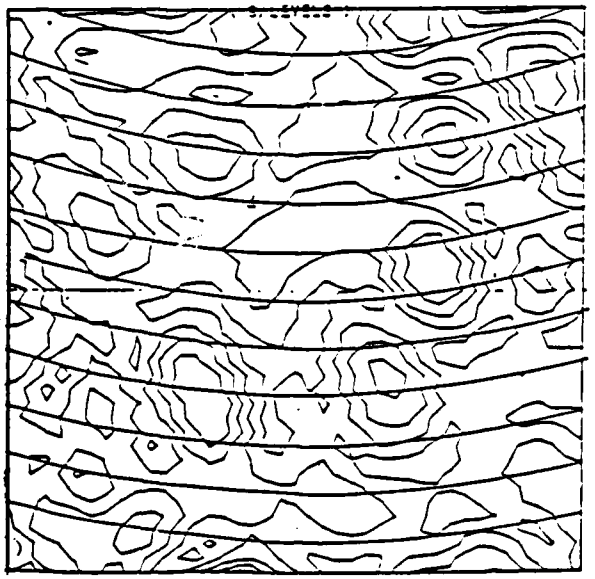

Figures 28 (a) - (c)
X-Y Scan Data on
Aluminum; Side-Mounted
Transducer

(a)

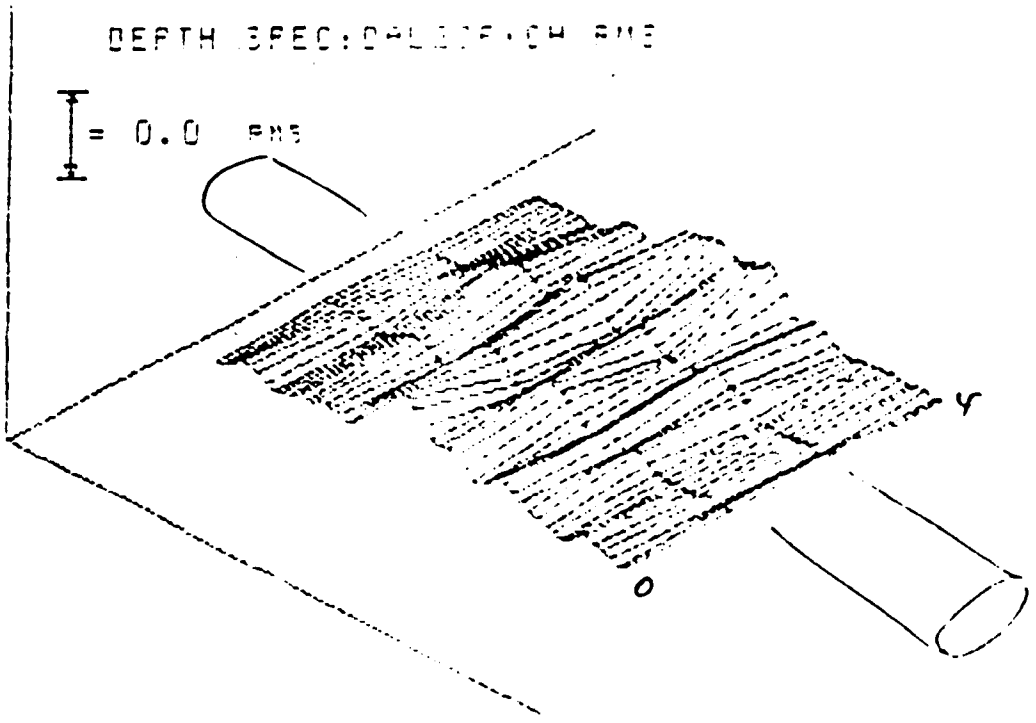

(b)

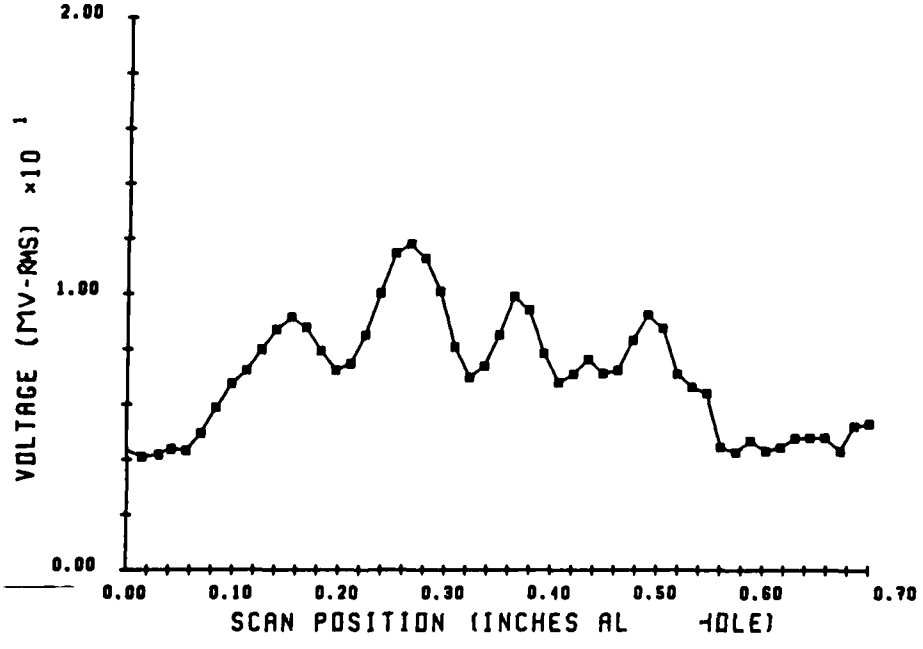

Figures 29 (a) - (b) - X-Y Scan of the Slanted Hole Aluminum Specimen.

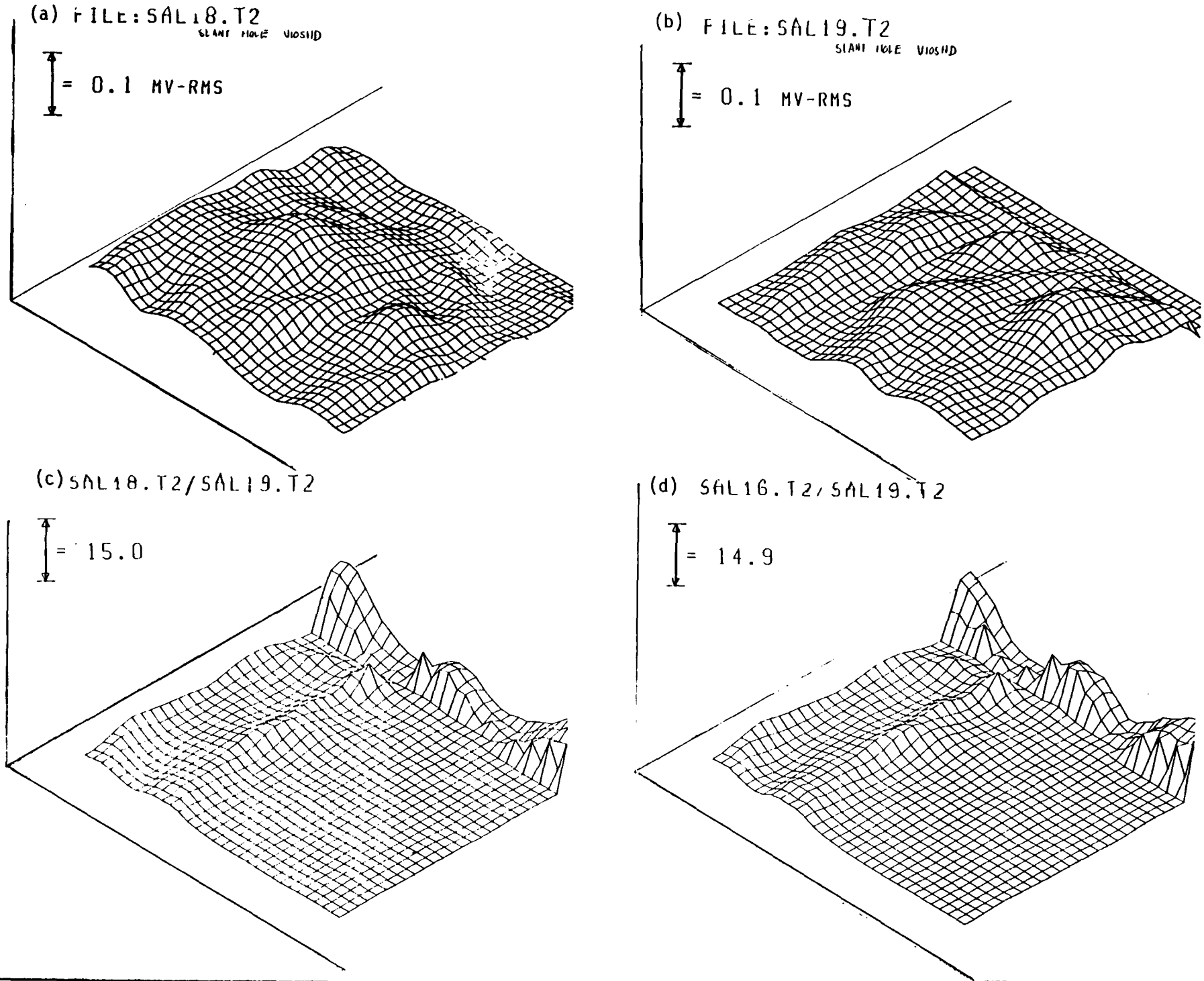
(a) FILE: SAL18.T2
SLANT HOLE VIOSHD
= 0.1 MV-RMS
(b) FILE: SAL19.T2
SLANT HOLE VIOSHD
= 0.1 MV-RMS
(c) SAL18.T2/SAL19.T2
= 15.0
(d) SAL16.T2/SAL19.T2
= 14.9

Figure 30 (a) - (d)

DTIC

END

4-86